Front. Phys. 11(5), 117103 (2016)
DOI 10.1007/s11467-016-0608-0

REVIEW ARTICLE

Strongly correlated Fermi systems as a new state of matter

V. R. Shaginyan[1,2,†], A. Z. Msezane[2], G. S. Japaridze[2], K. G. Popov[3], V. A. Khodel[4,5]

[1] *Petersburg Nuclear Physics Institute, NRC Kurchatov Institute, Gatchina, 188300, Russia*
[2] *Clark Atlanta University, Atlanta, GA 30314, USA*
[3] *Komi Science Center, Ural Division, RAS, Syktyvkar, 167982, Russia*
[4] *Russian Research Centre Kurchatov Institute, Moscow, 123182, Russia*
[5] *McDonnell Center for the Space Sciences & Department of Physics, Washington University, St. Louis, MO 63130, USA*
Corresponding author. E-mail: [†]*vrshag@thd.pnpi.spb.ru*
Received March 30, 2016; accepted July 12, 2016

The aim of this review paper is to expose a new state of matter exhibited by strongly correlated Fermi systems represented by various heavy-fermion (HF) metals, two-dimensional liquids like ^{3}He, compounds with quantum spin liquids, quasicrystals, and systems with one-dimensional quantum spin liquid. We name these various systems HF compounds, since they exhibit the behavior typical of HF metals. In HF compounds at zero temperature the unique phase transition, dubbed throughout as the fermion condensation quantum phase transition (FCQPT) can occur; this FCQPT creates flat bands which in turn lead to the specific state, known as the fermion condensate. Unlimited increase of the effective mass of quasiparticles signifies FCQPT; these quasiparticles determine the thermodynamic, transport and relaxation properties of HF compounds. Our discussion of numerous salient experimental data within the framework of FCQPT resolves the mystery of the new state of matter. Thus, FCQPT and the fermion condensation can be considered as the universal reason for the non-Fermi liquid behavior observed in various HF compounds. We show analytically and using arguments based completely on the experimental grounds that these systems exhibit universal scaling behavior of their thermodynamic, transport and relaxation properties. Therefore, the quantum physics of different HF compounds is universal, and emerges regardless of the microscopic structure of the compounds. This uniform behavior allows us to view it as the main characteristic of a new state of matter exhibited by HF compounds.

Keywords quantum phase transition, flat bands, non-Fermi-liquid states, strongly correlated electron systems, quantum spin liquids, heavy fermions, quasicrystals, thermoelectric and thermomagnetic effects, scaling behavior, new state of matter

PACS numbers 71.27.+a, 75.10.Kt, 71.23.Ft, 71.10.Pm, 71.10.Hf

Contents

1 Introduction 1
2 Extended quasiparticle paradigm and the scaling behavior of HF metals 2
2.1 Topological properties of systems with fermion condensate 3
2.2 Scaling behavior of HF metals 5
2.3 Universal behavior of the thermopower S_T of heavy-fermion metals 8
3 Two-dimensional ^{3}He 9
4 Quantum spin liquid 11
5 Quasicrystals 16
6 One-dimensional quantum spin liquid and other possible realizations of HF compounds 17
7 Summary 18
Acknowledgements 19
References and notes 19

1 Introduction

Strongly correlated Fermi systems are represented by a large variety of HF metals, insulators of new type with quantum spin liquids, quasicrystals, two-dimensional

*arXiv: 1608.02754.

(2D) systems and liquids like ^{3}He, and systems like $Cu(C_4H_4N_2)(NO_3)_2$ with one-dimensional (1D) quantum spin liquid. One can hardly expect these very different systems could exhibit a universal behavior that would allow one to view them as a new state of matter. We name these various systems HF compounds, for, as we shall see, they exhibit the behavior conforming to a type of HF metals. It is well known that three phase of matter exist: gaseous, liquid and solid, and at high enough temperatures any of these transforms into plasma - a system of chaotically moving nuclei and electrons with a gas-type behavior. Surprisingly, at the lower end of the temperature scale, close to the absolute zero such multi-particle systems as HF compounds exhibit universal behavior of their thermodynamic, transport and relaxation properties, that are governed by unique quantum phase transition called the fermion condensation quantum phase transition (FCQPT) that creates flat bands, and leads to the specific topological state known as the fermion condensate (FC). In this review we show both analytically and using arguments based entirely on the experimental grounds that all these HF compounds exhibit the universal scaling behavior formed by quasiparticles. This universal behavior, taking place at relatively low temperatures and induced by FCQPT, allows us to interpret it as the main feature of the new state of matter. Thus, whatever mechanism drives the system to FCQPT, the system demonstrates the universal behavior, despite numerous mechanisms or tuning parameters present at zero temperature, such as the pressure, number density, magnetic field, chemical doping, frustration, geometrical frustration, etc.

As we shall see in Section 2, at FCQPT the effective mass M^* of quasiparticles diverges; they survive FCQPT and define the thermodynamic, transport, and relaxation properties of HF compounds. Thus, quasiparticles form both the main properties and the universal scaling behavior, observed in HF compounds. Contrary to the Landau paradigm, where quasiparticles with approximately constant effective mass M^* are continuously linked with quasiparticles of non-interacting gas, the effective mass of the above new quasiparticles formed at FCQPT strongly depends on temperature T, magnetic field B, pressure P, and other external parameters. As a result, we introduce an extended quasiparticle paradigm, and show that new quasiparticles generate the non-Fermi liquid (NFL) behavior of the physical quantities of HF compounds, that are remarkably different from those of ordinary solids or liquids described by the Landau Fermi liquid (LFL) theory. Then, we briefly consider the topological properties of FC taking place beyond FCQPT, and how FCQPT generates the universal behavior of HF metals. We also discuss the experimental and pure theoretical arguments of the FC state.

The rest of the paper is organized as follows: In Sections 3, 4 and 5 we examine the universal scaling behavior of the thermodynamic, transport and relaxation properties of HF compounds represented by 2D ^{3}He, magnets of new types with quantum spin liquid (QSL) and the recently discovered quasicrystals, respectively, and show that HF compounds demonstrate the new state of matter. Section 6 presents a perspective of materials with 1D quantum spin liquid that can exhibit the properties of the new state of matter. Section 7 summaries the main results, placing the stress on the observation that the quantum physics of different strongly correlated Fermi systems is universal and emerges regardless of their underlying microscopic details. This uniform behavior, formed by flat bands, manifests the new state of matter.

2 Extended quasiparticle paradigm and the scaling behavior of HF metals

To analyze dependence of the effective mass M^* on temperature T, magnetic field B, momentum p, number density x, etc., we use the Landau equation for the effective mass [1–3]

$$\frac{1}{M^*(T,B)}=\frac{1}{M}+\int\frac{\boldsymbol{p_F}\boldsymbol{p_1}}{\boldsymbol{p_F^3}}F(\boldsymbol{p_F},p_1,n)\frac{\partial n(\boldsymbol{p_1},T,B)}{\partial \boldsymbol{p_1}}\frac{\mathrm{d}\boldsymbol{p_1}}{(2\pi)^3}, \tag{1}$$

where the Fermi–Dirac distribution reads

$$n_\pm(p,T,B)=\left\{1+\exp\left[\frac{\varepsilon(p,T)\pm B\mu_B-\mu}{T}\right]\right\}^{-1}. \tag{2}$$

Here, M is the bare mass, μ is the chemical potential, B is an external magnetic field, n is quasiparticle distribution function, and μ_B is the Bohr magneton. The term $\pm B\mu_B$ entering the right hand side of Eq. (2) describes Zeeman splitting. Equation (1) is exact and can be derived within the framework of the Density Functional Theory [4, 5]. This equation allows us to calculate the behavior of M^* which now becomes a function of temperature T, external magnetic field B, number density x, pressure P, etc. It is this feature of M^* that forms both the scaling and the non-Fermi liquid (NFL) behavior observed in measurements on strongly correlated Fermi systems [4–7]. In case of finite M^* and at $T=0$ the distribution function $n(p,T=0)$ becomes the step function $\theta(p_F-p)$, as it follows from Eq. (2), and Eq. (1) yields the well-known result

$$\frac{M^*}{M}=\frac{1}{1-F^1/3}, \tag{3}$$

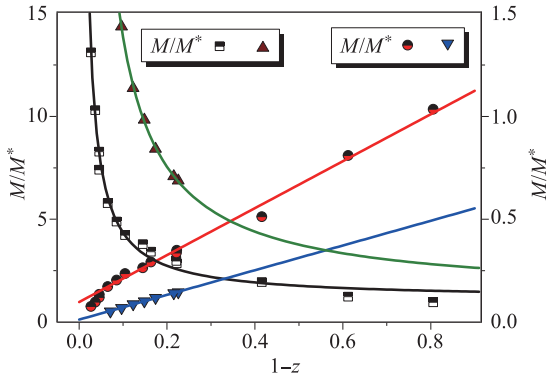

Fig. 1 The dependence of the effective mass $M^*(z)$ of 2D ^{3}He on dimensionless density $z = x/x_{FC}$. Experimental data from Ref. [10] are shown by circles and squares and those from Ref. [11] are shown by triangles. The effective mass M^*/M is fitted by Eq. (5), while the reciprocal $M/M^*(z) \propto a_3\, z$, where a_3 is a constant.

where $F^1 = N_0 f^1$, $f^1(p_F, p_F)$ is the p-wave component of the Landau interaction, p_F is the Fermi momentum, and $N_0 = M p_F/(2\pi^2)$ is the density of states (DOS) of a free Fermi gas. Because the number density $x = p_F^3/3\pi^2$, the Landau interaction can be written as $F^1(p_F, p_F) = F^1(x)$ [4]. At a certain critical point $x = x_{FC}$, with $x \to x_{FC}$ from below, the denominator $(1 - F^1(x)/3)$ tends to zero

$$(1-F^1(x)/3) \propto (x_{FC}-x)+a(x_{FC}-x)^2+\ldots \to 0, \quad (4)$$

and we find that

$$\frac{M^*(x)}{M} \simeq a_1 + \frac{a_2}{1 - x/x_{FC}} = a_1 + \frac{a_2}{1-z}, \quad (5)$$

where $x/x_{FC} = z$, a_1, and a_2 are constants, and $M^*(x \to x_{FC}) \to \infty$. As a result, at $T \to 0$ and $x \to x_{FC}$ the system undergoes a quantum phase transition [4, 5], represented by FCQPT. We note that the divergence of the effective mass given by Eq. (5) preserves the Pomeranchuk stability conditions, for F^1 is positive, rather than negative [6, 8, 9]. The divergence of the effective mass $M^*(x)$, given by (5) and observed in measurements on two-dimensional ^{3}He [10, 11], is illustrated in Fig. 1. It is seen that the calculations are in good agreement with the data [12].

2.1 Topological properties of systems with fermion condensate

The quasiparticle distribution function $n(p)$ of Fermi systems with FC is determined by the usual equation for a minimum of the Landau functional $E[n(p)]$. In contrast to common functionals of the number density x [13, 14], the Landau functional of the ground state energy E becomes functional of the occupation numbers n [4–6]. In case of homogeneous system a common functional becomes a function of $x = \sum_p n(p)$, while the Landau functional $E = E[n(p)]$ [4, 6, 15] satisfies

$$\frac{\delta E[n(p)]}{\delta n(p)} = \varepsilon(p) = \mu, \quad \text{when } 0 < n(p) < 1. \quad (6)$$

The minimum of the functional E has to be found from Eq. (6). While in the case of Bose system equation $\delta E/\delta n(p) = \mu$ is well established and understood, in case of Fermi system this equation, generally speaking, is not correct. It is the above constraint, $0 \le n(p) \le 1$, dictated by the Fermi distribution function that makes Eq. (6) applicable for Fermi systems. As we have seen above, in the case of LFL liquid at $T = 0$ the distribution function is represented by the step function: $n(p < p_F) = 1$ and $n(p > p_F) = 0$; while in the case of FC in some region of momenta, $p_i < p < p_f$, the distribution function becomes a smooth function at the Fermi surface, $0 < n(p) < 1$. Because of the above constraint, in the region $p_i < p < p_f$, Fermi quasiparticles can behave as Bose one, occupying the same energy level $\varepsilon = \mu$, and Eq. (6) yields the quasiparticle distribution function $n_0(p)$ that minimizes the ground-state energy E. Thus, at $T = 0$ the system undergoes a topological phase transition, for the Fermi surface at $p = p_F$ transforms into the Fermi volume for $p_i \le p \le p_f$ suggesting that at $T = 0$ the band is absolutely "flat" within this interval, giving rise to the spiky DOS as seen from the panel (a) of Fig. 2. A possible solution $n_0(p)$ of Eq. (6) and the corresponding single-particle spectrum $\varepsilon(p)$ are depicted in Fig. 2(b). As seen from the panel (b), $n_0(p)$ differs from the step function in the interval $p_i < p < p_f$, where $0 < n_0(p) < 1$, and coincides with the step function outside this interval. The existence of such flat bands, formed by inter-particle interaction, was predicted for the first time in Ref. [15]. Quasiparticles with momenta within the interval $(p_i < p < p_f)$ have the same single-particle energies equal to the chemical potential μ and form FC, while the distribution $n_0(p)$ describes the new state of the Fermi liquid with FC, and the Fermi system is split up into two parts: LFL and the FC part, as shown in Fig. 2(b) [4–6, 15–19].

The theory of fermion condensation permits the construction of new class of strongly correlated Fermi liquids with the fermion condensate [4, 6, 15–19]. In that case the quasiparticle system is composed of two parts: One of them is represented by FC located at the chemical potential μ, and giving rise to the spiky DOS, like that with $p = 0$ of Bose systems, as seen from Fig. 2(a), that shows the DOS of a Fermi liquid with FC located at the momenta $p_i < p < p_f$ and energy $\varepsilon = \mu$. Contrary to the condensate of a Bose system occupying the

$p = 0$ state, quasiparticles of FC with the energy $\varepsilon = \mu$ must be spread out over the interval $p_i < p < p_f$. Contrary to the Landau, marginal, superconducting LFL, or Tomonoga–Luttinger (marginal) Fermi liquids whose Green's functions exhibit the same topological behavior, in systems with FC, where the Fermi surface spreads into the Fermi volume, the Green's function belongs to a different topological class. The topological class of the Fermi liquid is characterized by the topological invariant [16–19]

$$N = \mathrm{tr} \oint_C \frac{\mathrm{d}l}{2\pi i} G(i\omega, p)\partial_l G^{-1}(i\omega, p), \tag{7}$$

where "tr" denotes the trace over the spin indices of the Green's function and the integral is calculated along an arbitrary contour C encircling the singularity of the Green's function. The invariant N in (7) assumes integer values even when the singularity is not a simple pole, cannot vary continuously, and is conserved in a transition from the Landau Fermi liquid to marginal liquids and under small perturbations of the Green's function. As shown by Volovik [16], the situation is quite different for systems with FC, where the invariant N becomes a half-integer and the system with FC transforms into an entirely new class of Fermi liquids with its own topological structure, preserving the FC state, and forming the new state of matter demonstrated by many HF compounds [5, 16–21].

In contrast to Bose liquid, whose entropy $S \to 0$ at temperature $T \to 0$, a Fermi liquid with FC possesses finite entropy S_0 at zero temperature [4, 22]. Indeed, as seen from Fig. 2(b), at $T = 0$, the ground state of a system with a flat band is degenerate, and the occupation numbers $n_0(p)$ of single-particle states belonging to the flat band are continuous functions of momentum p, in contrast to discrete standard LFL values 0 and 1. Such behavior of the occupation numbers leads to a T-independent entropy term $S_0 = S(T \to 0, n = n_0)$ with the entropy given by

$$S(n) = -\sum_p [n(p)\ln n(p) + (1-n(p))\ln(1-n(p))]. \tag{8}$$

Since the state of a system with FC is highly degenerate, FC triggers phase transitions that could lift the degeneracy of the spectrum and vanish S_0 in accordance with the Nernst theorem. For instance, FC can excite the formation of spin density waves, antiferromagnetic state, ferromagnetic state, the superconducting state, etc., thus strongly stimulating the competition between phase transitions eliminating the degeneracy. Contrary to LFL, where the entropy vanishes at zero temperature, the finite entropy S_0, characteristic of Fermi liquid with FC, causes the emergence of diversity of states. This observation is in accordance with the experimental phase

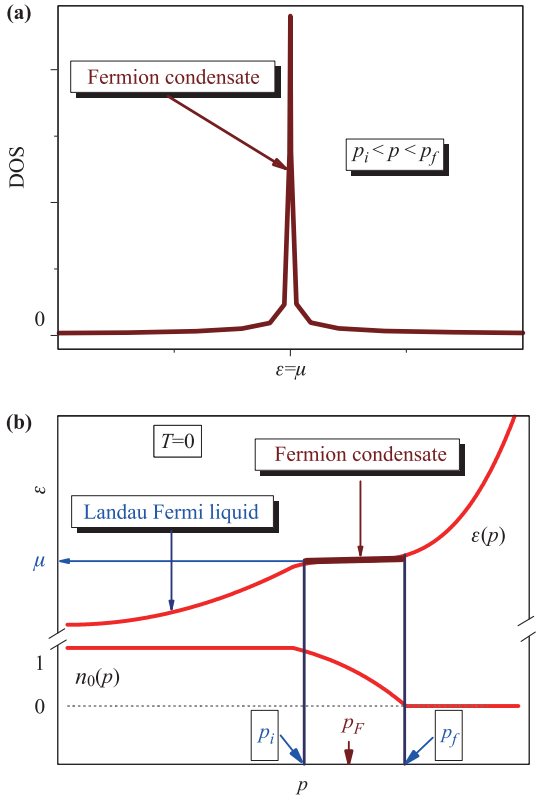

Fig. 2 Fermion condensate. **(a)** Schematic plot of the density of states (DOS) at low temperatures of quasiparticles versus ε at the momentum $p_i < p < p_f$ of a Fermi liquid with FC. **(b)** Schematic plot of two-component Fermi liquid at $T = 0$ with FC. The system is separated into two parts shown by the arrows: The first part is a Landau Fermi liquid with the quasiparticle distribution function $n_0(p < p_i) = 1$, and $n_0(p > p_f) = 0$; The second one is FC with $0 < n_0(p_i < p < p_f) < 1$ and the single-particle spectrum $\varepsilon(p_i < p < p_f) = \mu$. The Fermi momentum p_F satisfies the condition $p_i < p_F < p_f$.

diagrams [5, 23]. Since at $T = 0$ the entropy of ordered states is zero, we conclude that the entropy is discontinuous at the phase transition point, with its discontinuity $\delta S = S_0$. Thus, the entropy suddenly vanishes, with the system undergoing the first-order transition near which the critical quantum and thermal fluctuations are suppressed and the quasiparticles are well-defined excitations [4, 24]. As a result, we conclude that the main contribution to the transport and thermodynamic properties comes from quasiparticles rather than the various low energy boson excitations. We note that the existence of FC has been convincingly demonstrated by purely theoretical arguments, see, e.g., [4, 5, 18, 21, 25–27], and by experimental facts, see, e.g., [4, 5, 28, 29].

There are different kinds of instabilities of normal Fermi liquids connected with several perturbations of ini-

tial quasiparticle spectrum $\varepsilon(p)$ and occupation numbers $n(p)$, associated with the emergence of a multi-connected Fermi surface, see, e.g., [5, 16–19, 30]. Depending on the parameters and analytical properties of the Landau interaction, such instabilities lead to several possible types of restructuring of the initial Fermi liquid ground state. This restructuring generates topologically distinct phases. One of them is the FC, and the other belongs to a class of topological phase transitions, where the sequence of rectangles $n(p) = 0$ and $n(p) = 1$ is realized at $T = 0$, see, e.g., [31]. In fact, at elevated temperatures the systems located at these transitions exhibit behavior typical to those located at FCQPT. Therefore, we do not consider the specific properties of these topological transitions, but focus on the behavior of systems located near FCQPT.

2.2 Scaling behavior of HF metals

It is instructive to briefly explore the behavior of M^* in order to capture its universal behavior at FCQPT. Let us write the quasiparticle distribution function as $n_1(p) = n(p, T, B) - n(p)$, with $n(p)$ being the step function, Eq. (1) then becomes

$$\frac{1}{M^*(T,B)} = \frac{1}{M^*} + \int \frac{p_F p_1}{p_F^3} F(p_F, p_1) \frac{\partial n_1(p_1, T, B)}{\partial p_1} \frac{\mathrm{d}p_1}{(2\pi)^3}. \tag{9}$$

We now qualitatively analyze the solutions of Eq. (9) at $T = 0$. Application of magnetic field leads to Zeeman splitting of the Fermi surface, and the distance δp between the Fermi surfaces with spin up and spin down becomes $\delta p = p_F^{\uparrow} - p_F^{\downarrow} \sim \mu_B B M^*(B)/p_F$. We note that the second term on the right-hand side of Eq. (9) is proportional to $(\delta p)^2 \propto (\mu_B B M^*(B)/p_F)^2$, and therefore Eq. (9) reduces to [4]

$$\frac{M}{M^*(B)} = \frac{M}{M^*(x)} + c\frac{(\mu_B B M^*(B))^2}{p_F^4}, \tag{10}$$

where c is a constant. In the same way, one can calculate the change of the effective mass due to the variation of T [4]. For normal metals, where the electron liquid behaves like LFL with the effective mass of several bare electron masses $M^*/M \sim 1$, at temperatures even near 1000 K, the second term on the right hand side of Eq. (9) is of the order of T^2/μ^2 and is much smaller than the first term. The same is true, as can be verified, when a magnetic field of reasonable strength of $B \sim 100$ T is applied. Thus, the system behaves like LFL with the effective mass that is actually independent of the temperature or magnetic field, while the resistivity $\rho(T) \propto T^2$. This means that the correction to the effective mass determined by the second term on the right-hand side of Eq. (10) is small; thus the effective mass is approximatively constant under the influence of external parameters of reasonable strength. We recall that in the case of common metals $\mu \sim 1$ eV, therefore for reasonable temperatures T and magnetic fields B one obtain $T/\mu \ll 1$ and $\mu_B B/\mu \ll 1$. As a result, the integral on the right hand side of Eq. (1) represents a small correction to M^* as a function of T and B, provided that $M/M^* \sim 1$. At FCQPT, e.g., as soon as $x \to x_{FC}$, the effective mass $M^*(x)$ diverges and $M/M^*(x) \to 0$. In that case, the first term on the right hand side of Eq. (10) vanishes; the second term becomes principal, and determines M^* as a function of B. In the same way, Eq. (9) becomes homogeneous, and determines $M^*(T, B)$ as a universal function of temperature, magnetic field and other tuning parameters that drive the system to FCQPT. As it is seen from Figs. 3 (a) and (b), our observations are in accordance with the experimental facts: Under the application of low magnetic fields of 0.1 T the HF metal $YbRh_2Si_2$ exhibits LFL behavior at $T \simeq 0.1$ K, while the effective mass M^* is strongly dependent on both B and T. The only role of the Landau interaction F is to drive the system to FCQPT and the solutions of Eq. (9) are represented by some universal function of the variables T, B, x. In that case M^* strongly depends on the same variables. In contrast to the Landau quasiparticle paradigm that assumes approximate constancy of the effective mass, the extended quasiparticle paradigm is to be introduced. The main point here is that the well-defined quasiparticles determine as before the thermodynamic, relaxation and transport properties of strongly correlated Fermi-systems, while M^* becomes a function of T, B, x, etc. Moreover, the effective mass can be a divergent function of T, $M^*(T \to 0) \to \infty$ [4]. Thus, we have to introduce the modified and extended quasiparticles paradigm, that permits to naturally describe the basic properties and the scaling behavior of both the M^* and HF compounds. The essence of the paradigm is that in spite of the altering of Fermi surface topology the substance undergoes at FCQPT, the Landau quasiparticles survive but completely change their properties [4, 5, 30, 32].

A deeper insight into the behavior of $M^*(T, B)$ can be achieved by using some "internal" scales. Namely, near FCQPT the solutions of Eq. (9) exhibit a behavior such that $M^*(T, B)$ reaches its maximum value M^*_M at some temperature $T_M \propto B$ [4]. It is convenient to introduce the internal scales M^*_M and T_M to measure the effective mass and temperature. We rescale M^* and T by M^*_M and T_M. This generates the normalized dimensionless effective mass $M^*_N = M^*/M^*_M$ and the corresponding normalized dimensionless temperature $T_N = T/T_M$. As an illustration to the above consideration, we analyze the specific heat $C/T \propto M^*$ of the HF metal $YbRh_2Si_2$

[33]. When the magnetic field B is applied, the specific heat exhibits a behavior that is described by a function of both T and B. As seen from the panel (a) of Fig. 3, a maximum structure $(C/T)_M$ in $C/T \propto M_M^*$ at temperature T_M appears when B is applied. T_M shifts to higher T and $C/T \propto M_M^*$ diminishes as B is increased. The value of C/T reaches its maximum at lower temperatures, which decreases at elevated magnetic field. To obtain the normalized effective mass M_N^*, we use $(C/T)_M$ and T_M as "internal" scales: the maximum structure $(C/T)_M$ was used to normalize C/T, and T was normalized by T_M. In panel (b) of Fig. 3, the obtained $M_N^* = (C/T)/(C/T)_M = M^*/M_M^*$, as a function of normalized temperature $T_N = T/T_M$, is shown. It is seen that the LFL state with $M^* = const$ and NFL one are separated by the crossover at which M_N^* reaches its maximum value. The panel (b) of Fig. 3 reveals the scaling behavior of the normalized experimental curves: the curves at different magnetic fields B merge into a single one in terms of the normalized variable T/T_M. Our calculations of the normalized effective mass $M_N^*(T_N)$, shown by the solid line and based on Eq. (9), are in good agreement with the data [4, 5, 7, 34]. Near FCQPT the normalized solution of Eq. (1) $M_N^*(T_N)$ can be approximated well by a simple universal interpolating function [4]. The interpolation occurs between the LFL and NFL regimes and represents the universal scaling behavior of M_N^* [4, 34]

$$M_N^*(T_N) \approx c_0 \frac{1 + c_1 T_N^2}{1 + c_2 T_N^n}. \tag{11}$$

Here, $c_0 = (1+c_2)/(1+c_1)$, c_1, c_2 are fitting parameters; and the exponent $n = 8/3$ if the Landau interaction is an analytical function, otherwise $n = 5/2$ [4]. It follows from Eq. (9) that

$$T_M \simeq a_1 \mu_B B, \tag{12}$$

where a_1 is a dimensionless number. Equation (12) is in good agreement with experimental facts [35, 36], while possible corrections to Eq. (12), taking place near the corresponding phase transitions, are discussed in Refs. [5, 36]. Here we do not discuss these correction, for the main goal of our review is to expose the new state of matter exhibited by strongly correlated Fermi systems. Note that the effective mass M^* defines the thermodynamic properties of HF compounds, therefore $M^*(T) \propto C(T)/T \propto S(T)/T \propto M_0(T) \propto \chi(T)$ where $C(T)$ is the specific heat, $S(T)$ — entropy, $M_0(T)$ — magnetization and $\chi(T)$ — AC magnetic susceptibility. For the normalized values we have

$$M_N^* = (C/T)_N = (S/T)_N = (M_0)_N = \chi_N. \tag{13}$$

It is seen from Eq. (11) and Figs. 3 and 4, that at elevated temperatures the considered HF compounds exhibit the NFL behavior, $M^*(T) \propto T^{-2/3}$. NFL behavior

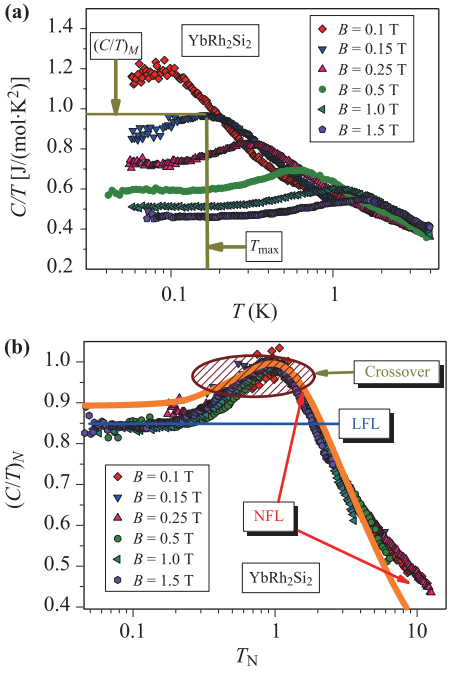

Fig. 3 Scaling behavior of HF metals. **(a)** Electronic specific heat of $YbRh_2Si_2$, C/T, versus temperature T as a function of magnetic field B [33] shown in the legend. The illustrative values of $(C/T)_M \propto M_M^*$ and T_M at $B = 0.15$ T are shown. **(b)** The normalized effective mass M_N^* versus normalized temperature T_N. M_N^* is extracted from the measurements of the specific heat C/T on $YbRh_2Si_2$ [33], displayed in the panel (a). The constant effective mass inherent in a normal Landau Fermi liquid is presented by the solid line. The schematic crossover region is indicated by the arrow and the NFL behavior is indicated by two arrows. Our calculation based on Eq. (1) is displayed by the solid curve.

manifests itself in the power-law behavior of the physical quantities of strongly correlated Fermi systems located close to their QCPs [37, 38], including QCPs related to metamagnetic phase transitions [39, 40], with exponents different from those of ordinary Fermi liquids. As seen from Figs. 4(a) and (b), M_N^* in different HF metals is the same, both in the high and low magnetic field. This observation is of utmost importance since allows us to verify the universal behavior in HF metals, when quite different magnetic fields are applied [4, 5, 41]. Relatively small values of M_N^* observed in $URu_{1.92}Rh_{0.08}Si_2$ and $CeRu_2Si_2$ at the high fields and small temperatures can be explained by taking into account that the narrow band is completely polarized. As a result, at low temperatures the summation over up and down spin projections reduces to a single direction producing the coefficient 1/2 in front of M_N^*, thus violating the scaling at low temperatures $T_N \leq 1$. At high temperatures the polarization vanishes and the summation is restored. As seen from Fig. 4(b), these observations are consistent with the ex-

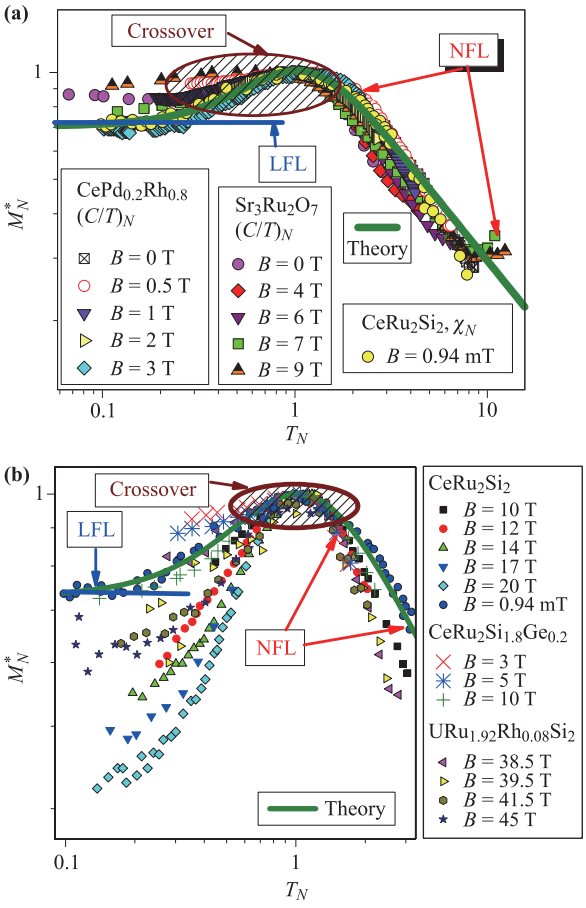

Fig. 4 The universal scaling behavior of the normalized effective mass M_N^* versus T_N. **(a)** M_N^* is extracted from the measurements of χ and C/T (in magnetic fields B shown in the legends) on $CeRu_2Si_2$ [37], $CePd_{1-x}Rh_x$ with $x = 0.80$ [33], and $Sr_3Ru_2O_7$ [38]. The LFL and NFL regimes (latter having $M_N^* \propto T_N^{-2/3}$) are shown by the arrows and straight lines. The transition regime is depicted by the shaded area. The solid curve represents our calculated universal behavior of $M_N^*(T_N)$. **(b)** The normalized effective mass versus the normalized temperature at different magnetic fields B, shown in the legend. $M_N^*(T_N)$ is extracted from measurements of C/T collected on $URu_{1.92}Rh_{0.08}Si_2$, $CeRu_2Si_2$ and $CeRu_2Si_{1.8}Ge_{0.2}$ at their metamagnetic phase transitions [39, 40]. The solid curve gives the universal behavior of M_N^*, Eq. (11).

perimental data collected in measurements under the application of high magnetic fields B on the archetypical HF metal $YbRh_2Si_2$ [42] the theoretical analysis of which is in good agreement with the experimental facts [41]. Thus, we conclude that different HF metals exhibit the same LFL, crossover and NFL behavior in strong magnetic fields that is in agreement with the notion of the new state of matter.

It is a common belief that the main output of theory is to explain the exponents that describe the NFL behavior, e.g., $C/T \propto T^q$, which are at least dependent on the magnetic character of QCP, dimensionality of the system, and employed scenario [43]. On contrary, the NFL behavior cannot be captured by these exponents as seen from Figs. 3 and 4. Indeed, the specific heat C/T exhibits a behavior that has to be described as a function of both temperature T and magnetic field B rather than by a single exponent. One can see that at low temperatures C/T demonstrates the LFL behavior which is changed by the crossover regime at which C/T reaches its maximum and finally C/T decays into NFL behavior as a function of T at fixed B. It is clearly seen from Figs. 3 and 4 that, in particularly in the transition regime, these exponents may have little physical significance. Thus, it is the quasiparticles of the extended paradigm that form the universal scaling behavior, and reproduce the salient experimental data [4, 5].

We note that there have been developed the Kondo breakdown theory, see, e.g., [44–46], the two-fluid description of heavy electron leading to quantum critical behavior, see, e.g., [47–49], and critical quasiparticle theory, see, e.g., [50, 51]. These perspective theories consider hybridization between conduction electrons and local magnetic moments, e.g., f orbitals, that produces a heavy electron liquid with an associated mass enhancement. As a result, one observes the itinerant heavy electron liquid in materials that contain a Kondo lattice of localized f electrons coupled to background conduction electrons. Thus, the Kondo effect in many materials develops quantum criticality that emerges from a competition between local moment magnetism and the conduction electron screening of the local moments [52, 53].

Interesting example of quantum criticality is represented by the heavy-fermion superconductor β-$YbAlB_4$: It is suggested that β-$YbAlB_4$ exhibits strange metallic (or NFL) behavior across an extensive pressure regime, distinctly separated from a high-pressure magnetic quantum phase transition by LFL phase [52, 53]. Moreover, the superconductor β-$YbAlB_4$ demonstrates the robustness of the NFL behavior of the thermodynamic properties and of the anomalous $T^{3/2}$ temperature dependence of the electrical resistivity under applied pressure in zero magnetic field B; such a behavior is at variance with the fragility of the NFL phase under application of tiny magnetic field [52, 53], strongly resembling the corresponding behavior observed in the quasicrystal $Au_{51}Al_{34}Yb_{15}$ [54, 55], as we shall see in Section 5. A consistent topological basis for this behavior observed in both the HF metal β-$YbAlB_4$ and the quasicrystal $Au_{51}Al_{34}Yb_{15}$, as well as the empirical scaling laws, may be found within the fermion-condensation theory [55, 56]. Then, as we shall see, the FC theory allows us to reveal and explain the universal behavior of two-dimensional liquids like ^{3}He, Section 3, compounds

with quantum spin liquids, Section 4, quasicrystals, Section 5, and systems with 1D quantum spin liquid, Section 6. Therefore, in our short review devoted to revealing the new state of matter, we employ the FC theory.

Several remarks concerning the applicability of Eqs. (1) and (11) to systems with violated translational invariance are in order. We study the universal behavior of HF metals, quantum spin liquids, and quasicrystals at low temperatures using the model of a homogeneous HF liquid [4, 5]. The model is applicable because we consider the scaling behavior exhibited by the thermodynamic properties of these materials at low temperatures, a behavior related to the scaling of quantities such as the effective mass M^*, the heat capacity $C/T \propto M^*$, the magnetic susceptibility $\chi \propto M^*$, etc. The behavior of $M^*_N(T_N)$, that is used to describe quantities mentioned above, is determined by momentum transfers that are small compared to momenta of the order of the reciprocal lattice length. The high momentum contributions can therefore be ignored by substituting the lattice with the jelly model. The values of the scales, like the maximum $M^*_M(B_0)$ of the effective mass measured at some field $B = B_0$ and T_M at which M^*_M emerges, are determined by a wide range of momenta. Thus, these scales are controlled by the specific properties of the system under consideration, while the scaled thermodynamic properties of different strongly correlated Fermi systems can be described by universal function (11) determining $M^*_N(T_N)$. It is seen from Figs. 3 and 4, and demonstrated by numerous experimental data collected on HF compounds that this observation is in a good agreement with experimental data [4, 5], and allows one to view the universal scaling behavior as a manifestation of the new state of matter exhibited by HF compounds.

2.3 Universal behavior of the thermopower S_T of heavy-fermion metals

In this section, we demonstrate that the thermopower S_T of such different heavy-fermion (HF) compounds as $YbRh_2Si_2$, β-$YbAlB_4$ and the strongly correlated layered cobalt oxide $[BiBa_{0.66}K_{0.36}O_2]CoO_2$ also exhibits the universal scaling behavior.

A study of the thermoelectric power S_T may deliver new insight into the nature of quantum phase transition that defines the features of new state of matter. For example, one may reasonably propose that the thermoelectric power S_T distinguishes between two competing scenarios for quantum phase transitions in heavy fermions, namely the spin-density-wave theory and the breakdown of the Kondo effect [57, 58]. Indeed, S_T is sensitive to the derivative of the density of electronic states and the change in the relaxation time at μ [3]. Using the Boltzmann equation, the thermopower S_T can be written as

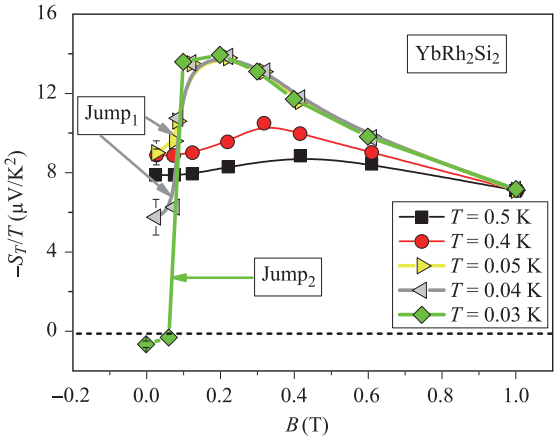

Fig. 5 Thermopower isotherm $-S_T(B)/T$ for different temperatures shown in the legend [62, 63]. The labels Jump_1 and Jump_2 represent the first and second downward jumps in $-S_T(B)/T$ shown by the arrows. The solid lines are guides to the eye.

[59–61]

$$S_T = -\frac{\pi^2 k_B^2 T}{3e}\left[\frac{\partial \ln \sigma(\varepsilon)}{\partial \varepsilon}\right]_{\varepsilon=\mu}, \tag{14}$$

where k_B and e are, respectively, the Boltzmann constant and the elementary charge, while σ is the dc electric conductivity of the system, given by

$$\sigma(\varepsilon) = 2e^2\tau(\varepsilon)\int \delta(\mu - \varepsilon(p))v(p)v(p)\frac{\mathrm{d}p}{(2\pi)^3}, \tag{15}$$

where p is the electron wave-vector, τ is the scattering time, and v denotes the velocities of electrons belonging to the bands crossing the Fermi surface at $\varepsilon = \mu$. Thus, we see from Eq. (15) that the thermoelectric power S_T is sensitive to the derivative of the density of electronic states $N(\varepsilon = \mu)$ and the change in the relaxation time at $\varepsilon = \mu$. On the basis of the Fermi liquid theory description, the term in the brackets on the right hand side of Eq. (14) can be simplified, so that one has $S_T \propto TN(\varepsilon = \mu) \propto C \propto M^*T$ at $T \to 0$ [59–61]. As a result, under general conditions and upon taking into account that charge and heat currents at low temperatures are transported by quasiparticles, the ratio $(S_T/C) \simeq const$ [59–61]. It is seen from Fig. 5 that in the case of $YbRh_2Si_2$ and at $T \geq T_{NL}$, the isotherms $-S_T(B)/T$ behave like C/T: They exhibit a broad maximum that sharpens and shifts to lower fields upon cooling [62, 63]. Here T_{NL} is the temperature of antiferromagnetic (AF) ordering ($T_{NL} = 70$ mK) at a critical field $B_{c0} = 60$ mT, applied perpendicular to the magnetically hard c axis [64]. Thus, $S_T/T \propto C/T \propto \chi \propto M^*$ over a wide range of T, since in the framework of FC theory, quasiparticles are responsible for the thermodynamic and

transport properties. It is worth noting that $S_T/T \propto M^*$ in a low-disorder two-dimensional electron system in silicon, and tends to a diverge at a finite disorder-independent density [65], thus confirming that the charge and heat currents are transported by quasiparticles.

To reveal the universal scaling behavior of the thermopower $S_T/T \propto C/T \propto M^*$, we normalize S_T/T in the same way as in the normalization of C/T: the normalized function $(S_T/T)_N$ is obtained by normalizing (S_T/T) by its maximum value, occurring at $T = T_M$, and the temperature T is scaled by T_M. Taking into account that $S_T/T \propto C/T$ [59–61], we conclude that $(S_T/T)_N = (C/T)_N = M_N^*$, provided that the system in question is located away from possible phase transitions. This universal function $(C/T)_N = M_N^*$ is displayed in Fig. 3(b). Figures 6(a) and (b) report $(S_T/T)_N$ as a function of the normalized magnetic field B_N and T_N, respectively. In Fig. 6(a), the function $(S_T/T)_N$ is obtained by normalizing (S_T/T) by its maximum occurring at B_M, and the field B is scaled by B_M. As seen from Eq. (11), the LFL behavior takes place at $B_N > 1$, since $(S_T/T)_N = M_N^*$, and $M_N^* \propto (B - B_{c0})^{-2/3}$ are T-independent, while at $B_N < 1$, M_M^* becomes T-dependent and exhibits the NFL behavior with $M_N^* \propto T_N^{-2/3}$. It is seen from Figs. 6(a) and (b) that the calculated values of the universal function M_N^* are in good agreement with the corresponding experimental data [62, 63, 66] over the wide range of the normalized magnetic field. Thus, $(S_T/T)_N$ exhibits the universal scaling behavior over a wide range of its scaled variable B_N and T_N. Figure 6(a) also depicts a violation of the scaling behavior for $B \leq B_{c0}$ when the system enters the AF phase. Moreover, as seen from Fig. 5 and Figs. 6(a) and (b), the scaling behavior is violated at $T \leq T_{NL}$ by two downward jumps. It is shown, these two jumps reflect the presence of flat band at μ in the single particle spectrum $\varepsilon(p)$ of heavy electrons in $YbRh_2Si_2$ [67]. In the same way, as it is seen from Fig. 6(b), the scaling behavior is violated by the superconducting (SC) phase transition, taking place in β-$YbAlB_4$ at $T_c = 80$ mK [66].

We now show that the observed scaling behavior of $(S_T/T)_N$ is universal by analyzing experimental data on the thermopower for $[BiBa_{0.66}K_{0.36}O_2]CoO_2$ [68]. By plotting $(S_T/T)_N$ as a function of T_N in Fig. 7, the universal scaling behavior and the three regimes are seen to be in a complete agreement with the reported overall behavior in both Figs. 3(b) and 4(a), and Figs. 6(a), (b) as well.

Thus, we have revealed and explained the universal scaling behavior of the thermopower S_T/T in such different HF compounds as $YbRh_2Si_2$, β-$YbAlB_4$, and $[BiBa_{0.66}K_{0.36}O_2]CoO_2$. Our calculations are in good agreement with experimental observations, and demonstrate that S_T/T exhibits the universal scaling behavior

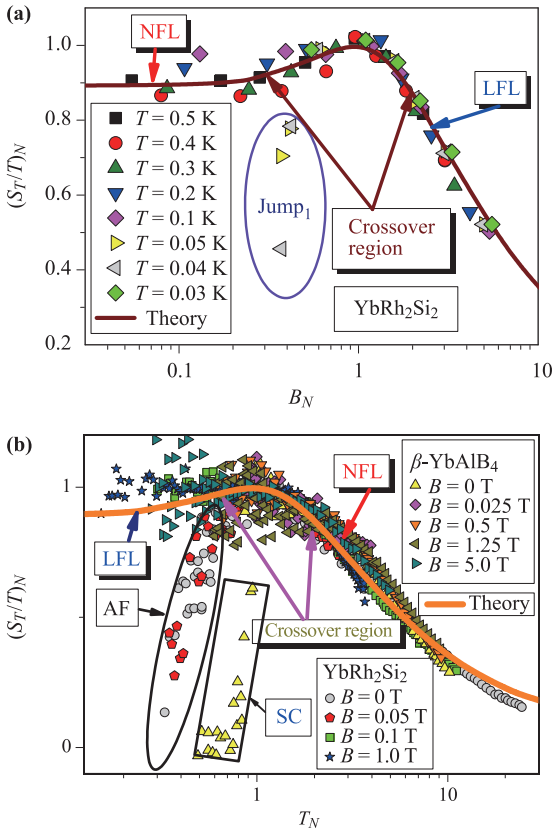

Fig. 6 **(a)** Normalized isotherm $(S_T(B)/T)_N$ versus normalized magnetic field B_N for different temperatures shown in the legend. The LFL behavior takes place at $B_N > 1$. **(b)** Temperature dependence of the normalized thermopower $(S_T/T)_N$ under several magnetic fields shown in the legend. The experimental data are extracted from measurements on $YbRh_2Si_2$ [62, 63] and on β-$YbAlB_4$ [66]. As it is explained in the text, the data, taken at the AF phase [62, 63] and at the superconducting one (SC) [66] and confined by both the ellipse and the rectangle, respectively, violate the scaling behavior. The solid curves in (a) and (b) represent calculated $(C/T)_N$ displayed in Fig. 3(b).

that characterizes and singles out the new state of matter.

3 Two-dimensional ^{3}He

In Section 2.2, it was discussed that the electronic system of HF metals demonstrates the universal low-temperature behavior irrespectively of their magnetic ground state. Therefore it is of crucial importance to check whether this behavior can be observed in 2D Fermi systems. Fortunately, the measurements on 2D ^{3}He are available [10, 11]. These measurements are extremely significant as they allow one to check for the universal behavior in the system formed by ^{3}He atoms, which are

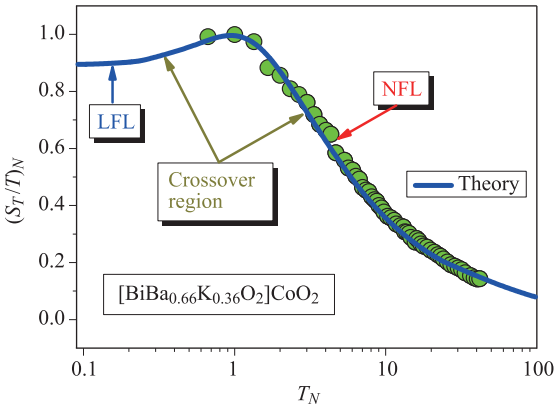

Fig. 7 Temperature dependence of $(S_T(T)/T)_N$ at magnetic field $B = 0$, extracted from measurements on $[BiBa_{0.66}K_{0.36}O_2]CoO_2$ [68], is displayed versus T_N. The solid line is the same as one depicted in Fig. 3(b).

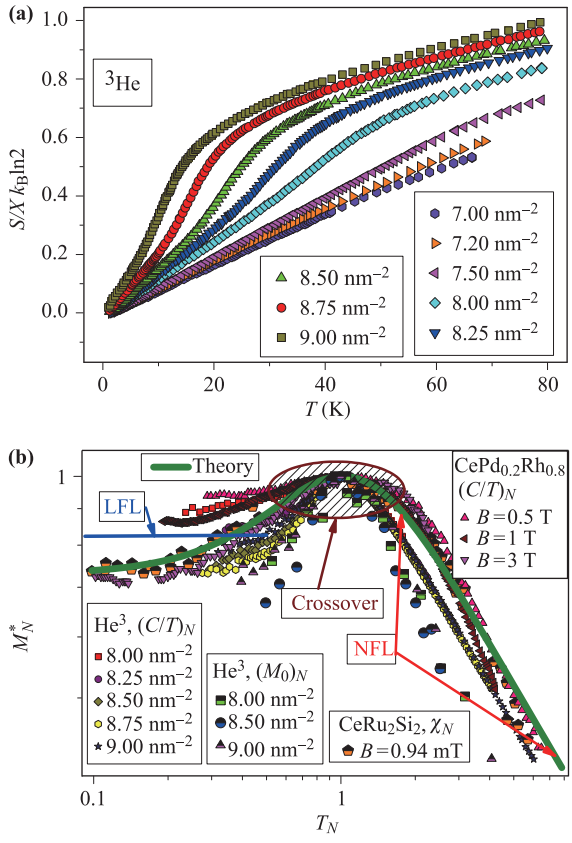

Fig. 8 Universal scaling of ^{3}He. **(a)** Temperature dependence of the entropy S of 2D ^{3}He at different densities x (shown in the legends) versus T [11]. **(b)** The normalized effective mass M_N^* as a function of the normalized temperature T/T_{max} is extracted from experimental data using Eq. (13). The behavior of M_N^* is extracted from experimental data for $S(T)/T$ in 2D ^{3}He [11] and 3D HF compounds with different magnetic ground states, such as $CeRu_2Si_2$ and $CePd_{1-x}Rh_x$ [33, 37], and fitted by the universal function (11).

essentially different from electrons [12]. Namely, atoms of 2D ^{3}He are neutral fermions with spin $S = 1/2$. They interact with each other by van-der-Waals forces with strong hardcore repulsion and a weakly attractive tail. The different character of interparticle interaction along with the fact, that the mass of ^{3}He atom is three orders of magnitude larger than that of an electron, makes ^{3}He to have drastically different microscopic properties than that of three-dimensional (3D) HF metals that constitute the most essential for our consideration. Because of this drastic difference one can not be sure that the macroscopic properties of the two fermion systems, mentioned above, will be similar. The bulk 3D liquid ^{3}He is historically the first object, to which the LFL theory has been applied. This substance, being intrinsically isotropic Fermi-liquid with negligible spin–orbit interaction is an ideal object to test the LFL theory. Unfortunately, FCQPT cannot be observed in 3D liquid ^{3}He, for it undergoes the first order phase transition under the application of pressure P long before some deviations from the LFL theory is observed. In contrast to 3D ^{3}He, its 2D counterpart exhibits strong deviations from the LFL theory as soon as its number density x approaches the critical density x_c, as it is seen from Fig. 8, panel (a). Thus, we can explore the behavior of 2D ^{3}He that is not hidden by possible phase transitions at $x < x_c$.

2D films of ^{3}He have been fabricated and thermodynamic properties have been thoroughly investigated [10, 11]. Among these properties are measurements of M^* as a function of the number density x and the entropy S as a function of x versus T, displayed in Figs. 1 and Fig. 8(a), respectively. We conclude that 2D ^{3}He is near FCQPT, since M^* diverges at $x \to x_c$, and at $x \gtrsim 7.50$ nm^{-2} the entropy is no more a linear function of temperature T, exhibiting the NFL behavior. Now we use the universal behavior of M_N^* given by Eq. (11) to fit the experimental data collected on both 2D ^{3}He and 3D HF metals [5]. M_N^*, extracted from the measurements on the ^{3}He film [11] at different densities $x < x_c$ smaller than at the critical point $x_c = 9.9 \pm 0.1$ nm^{-2} is reported in Fig. 8(b). In this panel, M_N^* extracted from the specific heat of ferromagnet $CePd_{0.2}Rh_{0.8}$ [33] and from AC magnetic susceptibility of paramagnet $CeRu_2Si_2$ [37] are plotted for different magnetic fields. It is seen that the universal behavior of M_N^* of 2D ^{3}He quasiparticles given by Eq. (11) [solid curve in Fig. 8(b)] is in agreement with experimental data. All the samples of 2D ^{3}He are located at $x < x_c$, where the system progressively disrupts its LFL behavior at elevated temperatures. In that case the control parameter, driving the system towards its critical point x_c, is merely the number density x. It is

seen that the behavior of M_N^*, extracted from measurements on 2D ^{3}He, is almost the same that of the 3D HF compounds [12]. We conclude that Eq. (11) allows us to reduce a four variable function describing the effective mass to a function of a single variable. Indeed, the effective mass depends on magnetic field, temperature, number density, and on the composition of the corresponding HF compound. It follows from our consideration that all these variables can be merged in the single variable by using Eq. (11). We conclude that despite absolutely different microscopic nature of 2D ^{3}He and 3D HF metals, they exhibit the new state of matter, demonstrating the universal scaling.

4 Quantum spin liquid

The first experimental observation of quantum spin liquid (QSL), supporting exotic spin excitations - spinons - and carrying fractional quantum numbers in the herbertsmithite $ZnCu_3(OH)_6Cl_2$, is reported in Ref. [69]. QSL can be viewed as an exotic quantum state composed of hypothetical particles such as fermionic spinons which carry spin 1/2 and no charge. The herbertsmithite $ZnCu_3(OH)_6Cl_2$ has been identified as a $S = 1/2$ Heisenberg antiferromagnet on a perfect kagome lattice, see Ref. [70] for a recent review. In $ZnCu_3(OH)_6Cl_2$, the Cu^{2+} ions with $S = 1/2$ form the triangular kagome lattice, and are separated by nonmagnetic intermediate layers of Zn and Cl atoms. The planes of the Cu^{2+} ions can be considered as two-dimensional (2D) layers with weak magnetic interactions along the third dimension. A simple kagome lattice has a dispersionless topologically protected branch of the spectrum with zero excitation energy that is the flat band [17, 71]. In that case FCQPT forms a strongly correlated quantum spin liquid (SCQSL) composed of fermions with zero charge, $S = 1/2$, and the effective mass $M_{\rm mag}^*$, occupying the corresponding Fermi sphere with the Fermi momentum p_F [72–75].

A comparison of the QSL specific heat $C_{\rm mag}/T \propto M_{\rm mag}^*$, extracted from measurements on $ZnCu_3(OH)_6Cl_2$ [72] with C/T of $YbRh_2Si_2$ [42, 73, 74], is shown in Figs. 9(a) and (b), respectively. As seen from Fig. 9(c), the QSL exhibits the scaling behavior similar to that of the electron liquid in HF metals under the application of magnetic fields [see Figs. 3(a), and Figs. 4(a), (b)] that lead to full polarization of the corresponding subband [5]. As a result, the specific heat becomes about half of that in small magnetic fields, as it is seen from Fig. 9(c) and Fig. 3(b) [5]. From the same figures one can see that the LFL, crossover and NFL regions are presented in both $ZnCu_3(OH)_6Cl_2$ and $YbRh_2Si_2$. The striking feature of the specific heat behavior is the strong dependence on the magnetic field seen from panels (a) and (b) of Fig. 9. Both $C_{\rm mag}/T$ of $ZnCu_3(OH)_6Cl_2$ and C/T of $YbRh_2Si_2$ exhibit the same qualitative and even quantitative behavior that allows us to view the herbertsmithite as insulator of new type with SCQSL, that occupies the Fermi sphere of a finite volume, as that of $YbRh_2Si_2$ occupied by heavy-electron liquid [41, 74–76]. It is worthy to note that the thermodynamic properties of $YbRh_2Si_2$ in strong magnetic fields can be explained within the frame of the FC theory [41], and these turn out to be similar to that of $ZnCu_3(OH)_6Cl_2$, as it is seen from Figs. 9(a), (b), and (c). We recall that at low temperatures the heat capacity of common insulators $C \propto T^3$, and $C/T \to 0$ that is in vivid contrast with the above experimental and theoretical observation.

Figure 10(a) displays the normalized spin-lattice relaxation rates $(1/T_1T)_N$ at fixed temperature versus normalized magnetic field B_N. It is seen from Fig. 10, that the magnetic field B progressively reduces $1/T_1T$, and the spin-lattice relaxation rate as a function of B possesses an inflection point at some $B = B_{inf}$ shown by the arrow. To clarify the universal scaling behavior of QSL in the herbertsmithite and in HF metals, we normalize both the function $1/T_1T$ and the magnetic field. Namely, we normalize $(1/T_1T)$ by its value at the inflection point, and the magnetic field is normalized by B_{inf}, $B_N = B/B_{inf}$. Since $(1/T_1T)_N = (M_N^*)^2$ [4, 77], we expect that different strongly correlated Fermi systems located near FCQPT will exhibit the same behavior of the normalized spin-lattice relaxation rate. It is seen from Fig. 10, that both the herbertsmithite $ZnCu_3(OH)_6Cl_2$ [78] and HF metal $YbCu_{5-x}Au_x$ [79] demonstrate similar behavior of the normalized spin-lattice relaxation rate. As seen from Fig. 10(a), at $B \leq B_{inf}$ (or $B_N \leq 1$), when the system is in its NFL region, the normalized relaxation rate $(1/T_1T)_N$ depends weakly on the magnetic field, while at higher fields, as soon as the system enters the LFL region, $(1/T_1T)_N = (M_N^*)^2 \propto B^{-4/3}$ diminishes in agreement with Eq. (11); in that case $n = 8/3$ [4, 5]. Figure 10(b) displays the normalized longitudinal magnetoresistance (LMR) ρ_N at fixed temperatures versus the normalized magnetic field B_N taken on the HF metal $YbRh_2Si_2$ [80]. Figure 10(b) shows that the growing magnetic field progressively reduces LMR, and it as a function of B it possesses an inflection point at $B = B_{inf}$ shown by the arrow. Both the normalized LMR and $(1/T_1T)_N$ obey the same equation [4, 5]

$$\frac{1}{(T_1T)_N} = \rho_N(B_N) = \frac{\rho_{LMR}(B_N) - \rho_0}{\rho_{inf}} = (M_N^*)^2 \propto B^{-4/3}, \quad (16)$$

where ρ_0 is the residual resistance, ρ_{inf} is LMR taken at the inflection point, ρ_{LMR} is LMR, ρ_N is the normalized LMR, and $B_N = B/B_{inf}$. We normalize LMR by their

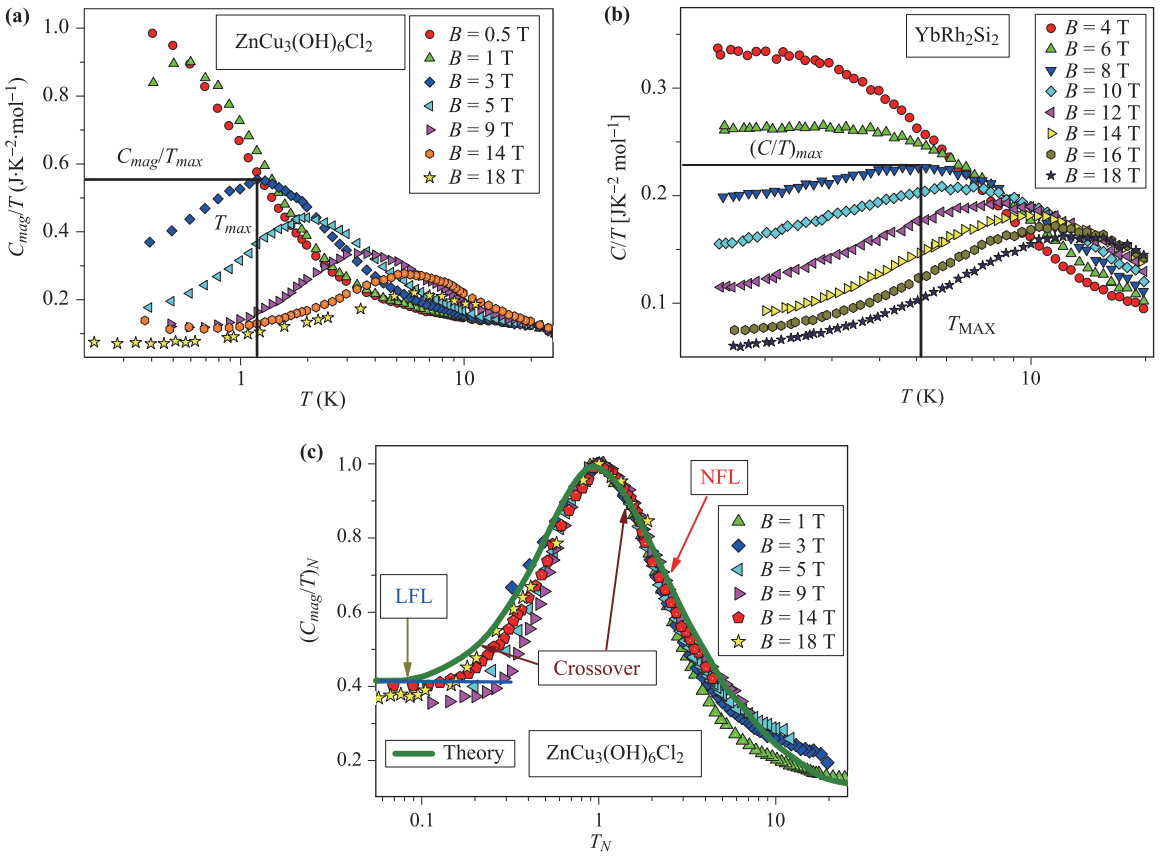

Fig. 9 The specific heat C_{mag}/T of the $ZnCu_3(OH)_6Cl_2$ insulator compared to that of the archetypical HF metal $YbRh_2Si_2$. **(a)** The specific heat $C_{\rm mag}/T$ of the QSL is extracted from measurements of the specific heat on $ZnCu_3(OH)_6Cl_2$ at different magnetic fields shown in the legend [42, 73]. **(b)** reports the T-dependence of the electronic specific heat C/T of $YbRh_2Si_2$ at different magnetic fields [42, 73] as shown in the legend. **(c)** Scaling behavior of the normalized specific heat $(C_{\rm mag}/T)_N$ extracted from the measurements shown in the panel (a). The LFL, crossover and NFL regions are shown by the arrows. The calculations are represented by the solid curve, describing the normalized effective mass M_N^* at high magnetic fields extracted from the specific heat (C/T) measurements of $YbRh_2Si_2$ shown in the panel (b) [41].

values at the inflection point, and the magnetic field is normalized by B_{inf}, as it has been done in the case of the spin-lattice relaxation rate. Thus, from Eq. (16) and Figs. 10(a) and (b), we conclude that the application of magnetic field B leads to the crossover from the NFL to LFL behavior and to the significant reduction in the relaxation rate and LMR, while both the normalized LMR and the normalized relaxation rate coincide, thus demonstrating the universal scaling behavior given by Eq. (11). From Fig. 10(c) it is clearly seen that the data collected on both $ZnCu_3(OH)_6Cl_2$ [81] and $YbRh_2Si_2$ [42] merge into the same curve, respecting scaling. This demonstrates that QSL of the herbertsmithite behaves like HF liquid of $YbRh_2Si_2$ in magnetic fields. Thus, SCQSL of $ZnCu_3(OH)_6Cl_2$ behaves like that of HF metals, and signals that the herbertsmithite demonstrates the new state of matter.

As mentioned above, QSL plays a role of HF liquid embedded into the insulating compound. Thus, we expect that the QSL in the herbertsmithite to behave like the electronic liquid in HF metals if the charge of an electron were zero. In that case, the thermal resistivity w of QSL is related to the thermal conductivity κ [82]

$$w = \frac{L_0 T}{\kappa} = w_0 + A_w T^2. \tag{17}$$

The thermal resistivity w behaves like the electrical resistivity $\rho = \rho_0 + A_\rho T^2$ of the electronic liquid, since A_w represents the contribution of spinon-spinon scattering to the thermal transport, being analogous to the contribution A_ρ to the charge transport induced by electron-electron scattering. Here, L_0 is the Lorenz number, ρ_0 and w_0 are residual resistivity of electronic liquid and QSL, respectively, and the coefficients are $A_w \propto (M^*_{\rm mag})^2$ and $A_\rho \propto (M^*)^2$. Thus, we expect that in the LFL region A_w of the thermal resistivity of QSL under the application of magnetic fields at fixed T to behave like $(1/T_1T)_N$ and ρ_N shown respectively in Figs. 10(a)

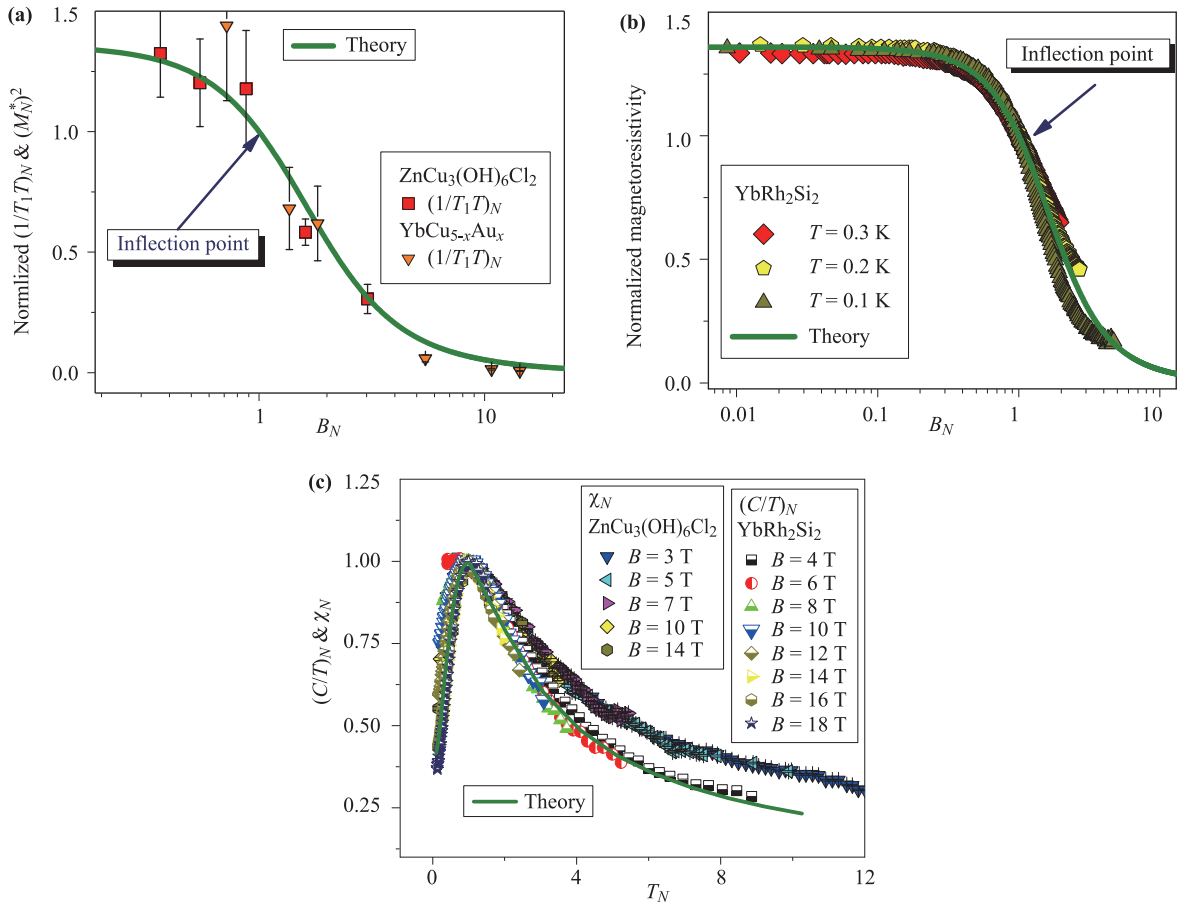

Fig. 10 Relaxation, transport and thermodynamic properties of QSL. **(a)** comparison of the relaxation properties of the herbertsmithite with those of a HF metals. The normalized spin-lattice relaxation rate $(1/T_1T)_N$ at fixed temperature as a function of magnetic field: Solid squares correspond to data on $(1/T_1T)_N$ extracted from measurements on $ZnCu_3(OH)_6Cl_2$ [78], while the solid triangles correspond to those extracted from measurements on $YbCu_{5-x}Au_x$ with $x = 0.4$ [79]. The inflection point, representing the crossover region where the normalization is taken, is shown by the arrow. Our calculations based on Eqs. (9) and (11) are depicted by the solid curve, tracing the scaling behavior of $(M_N^*)^2$. **(b)** The normalized longitudinal magnetoresistance ρ_N versus B_N. ρ_N is extracted from measurements on $YbRh_2Si_2$ at different temperatures [80] that are listed in the legend. The solid curve represents our calculations and coincides with that shown in the panel (a). **(c)** The normalized effective mass M_N^* extracted from measurements of susceptibility χ [81] on $ZnCu_3(OH)_6Cl_2$ and (C/T) on $YbRh_2Si_2$ [42]. Our calculations of M_N^* are shown by the solid curve.

and (b), namely $A_w \propto (1/T_1T)_N \propto \rho_N \propto (M^*(B)_{\rm mag})^2$. However, in the LFL region at fixed magnetic fields the thermal conductivity κ is a linear function of temperature, $\kappa \propto T$ [82].

The study of the thermal resistivity w given by Eq. (17) leads to revelation of spinons as itinerant excitations. The temperature dependence of thermal resistivity w represented by the finite term w_0 demonstrates that the behavior of QSL is similar to that of metals, and there is a finite residual term κ/T in the zero-temperature limit of κ. The presence of this term immediately establishes that there are gapless excitations, associated with the property of normal metals, in which gapless electrons govern the heat transport. The finite w_0 implies that in QSL both k/T and $C_{mag}/T \propto M^*_{\rm mag}$ remain nonzero as $T \to 0$. Therefore, gapless spinons, forming the Fermi surface, govern the specific heat and the transport. Key information on the nature of spinons is further provided by the B-dependence of the coefficient A_w. The specific B-dependence of the resistivity $w(B) \propto (M^*_{\rm mag})^2$, given by Eq. (16), would establish the behavior of QSL as SCQSL. We note that the heat transport is polluted by the phonon contribution. On the contrary, the phonon contribution is hardly influenced by magnetic field B. Therefore, we expect the B-dependence of the heat conductivity to be governed

by $A_w(B,T)$. Consider the approximate relation,

$$1-\frac{A_w(B,T)}{A_w(0,T)} = 1-\left(\frac{M^*(B,T)_{\rm mag}}{M^*(0,T)_{\rm mag}}\right)^2 \simeq a(T)\frac{\kappa(B,T)-\kappa(0,T)}{\kappa(0,T)} \equiv a(T)I(B,T), \quad (18)$$

where the coefficient $a(T)$ is B-independent. To derive (18), we use Eq. (17), and obtain [5, 82]

$$\frac{\kappa}{L_0T} = \frac{1}{w_0+A_wT^2}+bT^2. \quad (19)$$

Here, the term bT^2 describes the phonon contribution to the heat transport. Upon carrying out simple algebra and assuming that $[1-A_w(B,T)/A_w(0,T)] \ll 1$, we arrive at Eq. (18). From Fig. 10(a) and (b), it is seen that the effective mass $M_N^*(B) \propto M_{\rm mag}^*(B)$ is a decreasing function of the magnetic field B. Then, it follows from Eqs. (16) and (18) that the function $I(B,T) = [\kappa(B,T)-\kappa(0,T)]/\kappa(0,T)$ increases with B increasing.

Recent measurements of $\kappa(B)$ on the organic insulators $EtMe_3Sb[Pd(dmit)_2]_2$ and κ-$(BEDT-TTF)_2Cu_2(CN)_3$ [83, 84] are displayed in Fig. 11(a) and (b). The measurements show that the heat is carried by phonons and QSL, since the heat conductivity is well fitted by $\kappa/T = a_1 + a_2T^2$, where a_1 and a_2 are constants. The finite term a_1 implies that spinon excitations are gapless in $EtMe_3Sb[Pd(dmit)_2]_2$, while in κ-$(BEDT-TTF)_2Cu_2(CN)_3$ gapless excitations are still being debated [84]. A simple estimation indicates that the ballistic propagation of spinons appears to be realized in the case of $EtMe_3Sb[Pd(dmit)_2]_2$ [83, 84]. From Fig. 11(a) and (b), the normalized data $I(B,T) = [\kappa(B,T)-\kappa(B=0,T)]/\kappa(B=0,T)$ demonstrates a strong B-dependence, namely the field dependence shows an increase of thermal conductivity for increasing B. Such behavior is in agreement with Eq. (16) and Fig. 10(a); it demonstrates that $(M^*(B)_{mag})^2$ is a decreasing function of B. Consequently, it is seen from Eq. (18), that $I(B,T)$ is an increasing function of B. It is seen from Figs. 11(a) and (b), that $I(B,T)$ as a function of B possesses an inflection point at some $B=B_{inf}$. To reveal the scaling behavior of QSL in both $EtMe_3Sb[Pd(dmit)_2]_2$ and κ-$(BEDT-TTF)_2Cu_2(CN)_3$, we normalize both the function $I(B,T)$ and the magnetic field by their values at the inflection points, as it was done in the case of $(1/T_1T)$, see Fig. 10(a). In that case we eliminate factor $a(T)$, appearing in Eq. (18), and our calculations are free of any fitting parameters. Moreover, the theoretical curve shown in Figs. 11(a) and (b), is extracted from those shown in Figs. 10(a) and (b), and, thus, is defined by LMR measured on $YbRh_2Si_2$ and by $(1-(1/T_1T)_N)$ extracted from measurements of the spin relaxation rate on $ZnCu_3(OH)_6Cl_2$ and $YbCu_{5-x}Au_x$. Clearly, from Fig. 11, the normalized $I_N(B_N,T)$ exhibits the scaling behavior and becomes a function of a single variable B_N, yielding good overall agreement between our calculations and the experimental data [83, 84].

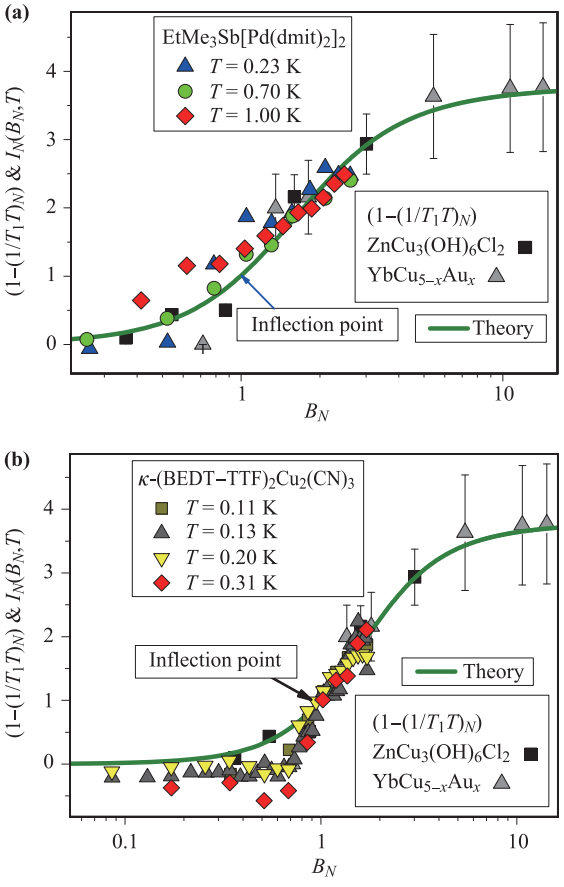

Fig. 11 Normalized thermal conductivity $I_N(B_N,T)$ of the organic insulators. **(a)** $I_N(B_N,T)$ measured on $EtMe_3Sb[Pd(dmit)_2]_2$ as function of the normalized magnetic field B_N at temperatures shown in the legend [83, 84]. The inflection point is shown by the arrow. Our calculations based on Eq. (18) are represented by the solid curve. **(b)** $I_N(B_N,T)$ measured on κ-$(BEDT-TTF)_2Cu_2(CN)_3$ as function of the normalized magnetic field B_N at temperatures shown in the legend [83, 84]. The inflection point is shown by the arrow. In both panels, the data $(1-(1/T_1T)_N)$ extracted from measurements of the spin relaxation rate on $ZnCu_3(OH)_6Cl_2$ and $YbCu_{5-x}Au_x$, see Fig. 10(a), are shown by the filled squares and triangles. Our calculations based on Eq. (18) are indicated by the solid curve that is obtained from the theoretical curve shown in Figs. 10(a) and (b) [82].

Neutron scattering measurements of the dynamic spin susceptibility $\chi(q,\omega,T) = \chi'(q,\omega,T) + i\chi''(q,\omega,T)$, as a function of momentum q, frequency ω and temperature T, play important role when identifying the properties of quasiparticles. At low temperatures, such mea-

surements reveal that quasiparticles excitations of the new type insulators are represented by spinons, form a continuum, and populate an approximately flat band crossing the Fermi level [69]. In that case it is expected that the normalized susceptibility $(T^{2/3}\chi'')_N$ exhibits scaling as a function of the dimensionless variable E_N [5, 76]. As was done for M_N^* when constructing Eq. (11), we introduce the dimensionless function $(T^{2/3}\chi'')_N = T^{2/3}\chi''/(T^{2/3}\chi'')_{\max}$ and the dimensionless variable $E_N = E/E_{\max}$; then the equation describing the normalized susceptibility $(T^{2/3}\chi'')_N$ reads

$$(T^{2/3}\chi'')_N \simeq \frac{b_1 E_N}{1 + b_2 E_N^2}, \tag{20}$$

with b_1 and b_2 being fitting parameters which are adjusted so that the function $(T^{2/3}\chi'')_N$ reaches its maximum value 1 at $E_n = 1$ [5, 76]. The panel (a) of Fig. 12 reports $(T^{2/3}\chi'')_N$ extracted from measurements of the inelastic neutron scattering spectrum on the HF metal $Ce_{0.925}La_{0.075}Ru_2Si_2$ [85]. The scaled data obtained in measurements on such a quite distinct strongly correlated systems as $ZnCu_3(OH)_6Cl_2$ [81] and the deuteronium jarosite $(D_3O)Fe_3(SO_4)_2(OD)_6$ [86] are shown in the panel (b) and (c). It is seen that our calculations shown by the solid curves are in good agreement with the experimental data collected on $Ce_{0.925}La_{0.075}Ru_2Si_2$, $ZnCu_3(OH)_6Cl_2$ and $(D_3O)Fe_3(SO_4)_2(OD)_6$ over almost three orders of the scaled variable E_N and $(T^{2/3}\chi'')_N$ does exhibit the scaling behavior. Thus, the spin excitations in both $ZnCu_3(OH)_6Cl_2$ and $(D_3O)Fe_3(SO_4)_2(OD)_6$ demonstrate the same itinerate behavior as electron excitations of the HF metal $Ce_{0.925}La_{0.075}Ru_2Si_2$ do, and, therefore form a continuum. This observation of the continuum is of great importance since it clearly reveals the presence of QSL in the herbertsmithite [76, 87]; this was later

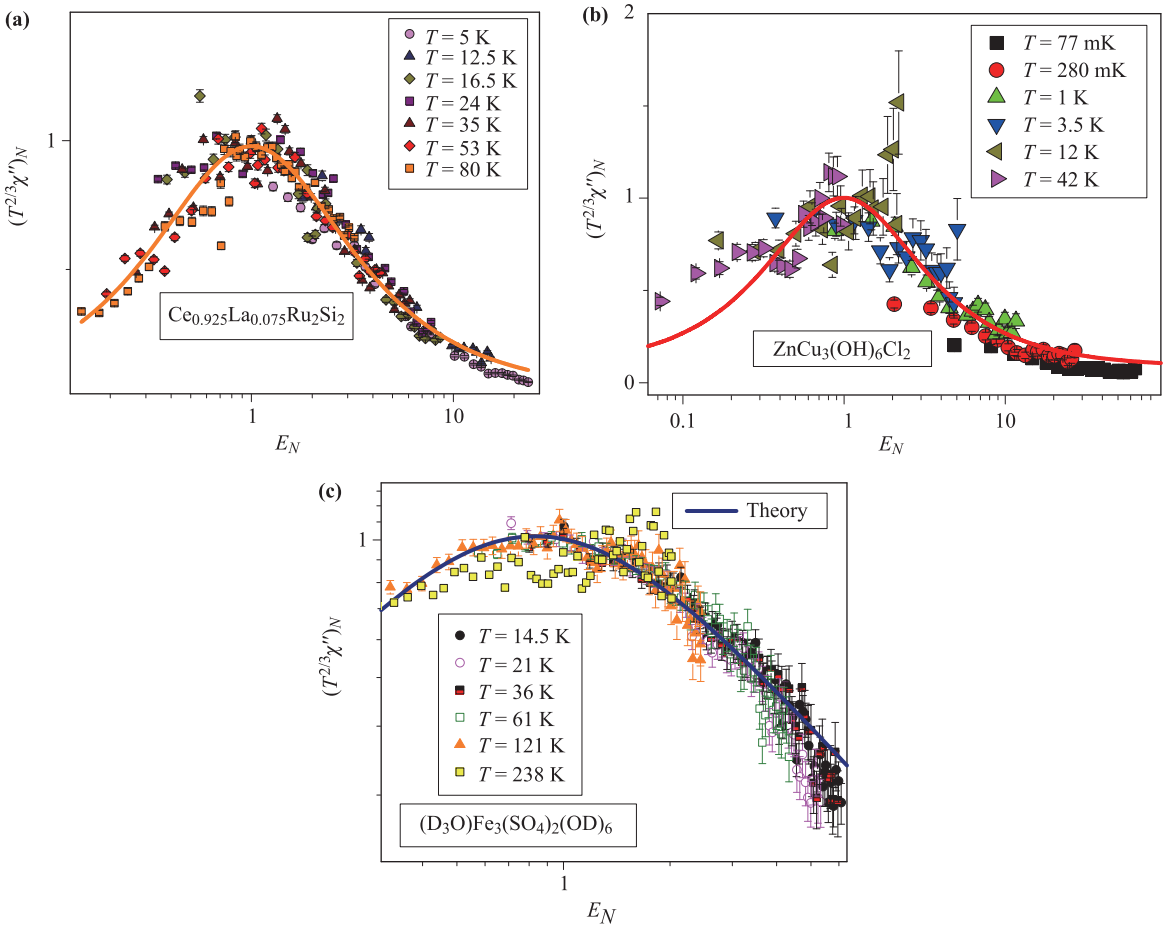

Fig. 12 The scaling behavior of the normalized dynamic spin susceptibility $(T^{2/3}\chi'')_N$. **(a)** $(T^{2/3}\chi'')_N$ plotted against the dimensionless variable E_N. The data are extracted from measurements on the HF metal $Ce_{0.925}La_{0.075}Ru_2Si_2$ [85]. **(b)** $(T^{2/3}\chi'')_N$ versus E_N. The data are extracted from measurements on the herbertsmithite $ZnCu_3(OH)_6Cl_2$ [81]. **(c)** $(T^{2/3}\chi'')_N$ versus E_N. The data are extracted from measurements on the deuteronium jarosite $(D_3O)Fe_3(SO_4)_2(OD)_6$ [86]. For all these HF compounds our calculations, based on Eq. (20), are shown by the solid curves [76].

confirmed by direct experimental observation [69].

Thus, the non-Fermi liquid behavior and the scaling properties of such strongly correlated Fermi systems as insulators $ZnCu_3(OH)_6Cl_2$, $(D_3O)Fe_3(SO_4)_2(OD)_6$, $EtMe_3Sb[Pd(dmit)_2]_2$, κ-$(BEDT-TTF)_2Cu_2(CN)_3$, and HF metals $Ce_{0.925}La_{0.075}Ru_2Si_2$, $YbCu_{5-x}Au_x$, and $YbRh_2Si_2$ are described within the framework of the theory of FC, and their scaled thermodynamic, transport and relaxation properties are governed by Eqs. (11) and (20). Our calculations are in a good agreement with the experimental data, and allow us to identify the low-temperature behavior of $ZnCu_3(OH)_6Cl_2$, $(D_3O)Fe_3(SO_4)_2(OD)_6$, κ-$(BEDT-TTF)_2Cu_2(CN)_3$, and $EtMe_3Sb[Pd(dmit)_2]_2$ as determined by SCQSL. The same behavior is observed in other HF compounds like HF metals and 2D ^{3}He. Thus, HF compounds with QSL can be viewed as a new type of strongly correlated electrical insulators that form the new state of matter and possess the properties and the universal scaling behavior of HF metals with one exception: it resists the flow of electric charge, but supports the spin current formed by spinons.

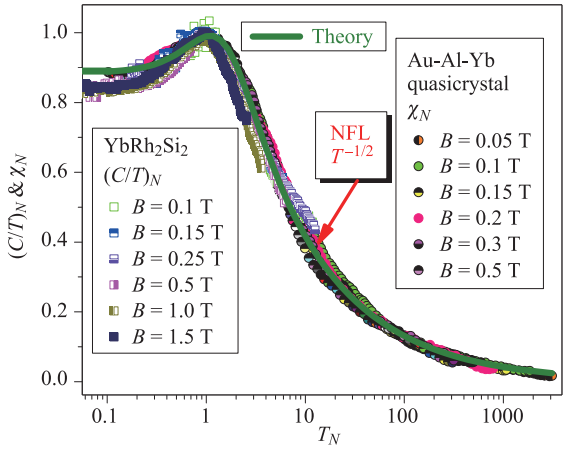

Fig. 13 The normalized specific heat $(C/T)_N$ and the normalized magnetic susceptibility χ_N extracted from measurements in magnetic fields B on the HF metal $YbRh_2Si_2$ [33] and on the quasicrystal $Au_{51}Al_{34}Yb_{15}$ [54], respectively. The corresponding magnetic fields are listed in the legends. The arrow shows the $T^{-1/2}$ regime taking place at $T_N > 1$. Our calculations are represented by the solid curve tracing the scaling behavior of $(C/T)_N = \chi_N = M_N^*$ given by Eq. (11).

5 Quasicrystals

The study of new materials dubbed quasicrystals (QCs) and characterized by noncrystallographic rotational symmetry and quasiperiodic translational properties have continued from quite some time [88]. Study of such extraordinary HF compounds as quasicrystals may shed light on the most basic features related to the universal behavior observed in HF compounds. Experimental measurements on the gold-aluminium-ytterbium quasicrystal $Au_{51}Al_{34}Yb_{15}$ have revealed a specific behavior with the unusual exponent $\beta \simeq 0.51$ defining the divergency of the magnetic susceptibility $\chi \propto T^{-\beta}$ at $T \to 0$ [54]. The measurements have also revealed that the observed NFL behavior transforms into that of the LFL with application of a tiny magnetic field B. All these facts challenge theory to explain the unique properties of the gold-aluminum-ytterbium QC. In case of QCs electrons occupy a new class of states denoted as "critical states", neither being extended nor localized. Associated with these critical states, characterized by an extremely degenerate confined wave function, are the so-called "spiky" DOS [89]. These predicted DOS are corroborated by experiments revealing the spiky DOS [90], which are formed by flat bands [91]. As a result, we conclude that the electronic system of some quasicrystals is located at FCQPT without tuning [5, 55].

We now investigate the behavior of χ as a function of temperature at fixed magnetic fields. The effective mass $M^*(T,B)$ can be extracted from the data since $M^*(T,B) \propto \chi$, see Eq. (13). If the corresponding measurements are carried out at fixed magnetic field B, then, as it follows from the Eq. (11), χ reaches the maximum χ_M at some temperature T_M. Upon normalizing both χ and the specific heat C/T by their peak values at each value of magnetic field B and the corresponding temperatures by T_M, we observe from Eq. (11) that all the curves merge into a single one, thereby demonstrating the scaling behavior typical for HF metals [4]. As seen from Fig. 13, χ_N extracted from measurements on $Au_{51}Al_{34}Yb_{15}$ [54] exhibits the scaling behavior given by Eq. (11) and our calculations agree well with the data over four orders of magnitude in normalized temperature. Also seen is that χ_N agrees well with the normalized $(C/T)_N$ extracted from measurements in magnetic fields on $YbRh_2Si_2$ [33]. At $T_N > 1$ the susceptibility $\chi_N(T) \propto T^{-\beta}$, with $\beta = 1/2$. It is seen from Figs. 13 and 14, panel (b), that the $T^{-\beta}$ regime with $\beta = 1/2$ is marked as NFL since contrary to the LFL case, the effective mass depends strongly on temperature. Additionally, it is observed the robustness of the NFL phase against application of pressure P in zero magnetic field, in that the divergent T and B dependencies of χ are conserved [54]. In contrast to resilience of these divergences under pressure, application of even a tiny magnetic field B is sufficient to suppress them, leading to Landau Fermi liquid (LFL) behavior at low temperatures, as we have seen above. Thus, the paramagnetic NFL phase of $Au_{51}Al_{34}Yb_{15}$ takes place without magnetic criticality, and not from quantum critical fluctu-

ations, strongly resembling the corresponding behavior observed in β-$YbAlB_4$ [55, 56].

Again, we conclude that the QC $Au_{51}Al_{34}Yb_{15}$ belongs to the family of HF compounds, and, thus, demonstrates the new state of matter.

6 One-dimensional quantum spin liquid and other possible realizations of HF compounds

We have shown above that different HF compounds exhibit the uniform and universal scaling in their thermodynamic, transport and relaxation properties in the wide range of magnetic field, temperature, number density, etc. Additionally to the already known materials whose properties provide information on both the existence of FCQPT and the new state of matter, there exists a variety of other objects of great interest; these could be studied and understood within the framework of the FC theory and flat bands. Among such objects are neutron stars, atomic clusters and fullerenes, ultra cold gases in traps, 1D quantum spin systems, and the Universe itself [4, 5, 92–94].

In 1D quantum spin liquid FCQPT plays a role of QCP taking place at $H = H_s$. Here H_s is the saturation magnetic field, where QCP occurs, for near QCP taking place at $H = H_s$ and $T = 0$, the fermion spectrum becomes almost flat, and the fermion (spinon) effective mass diverges, $M^* \propto M/p_{FH} \to \infty$, due to kinematic mechanism, since the Fermi momentum $p_{FH} \to 0$ of becoming empty subband [95, 96]. In other words, at $H = H_s$ both antiferromagnetic sublattices align in the field direction i.e. the magnetic field fully polarizes the spins; at $H \geq H_s$ the ground state is a gapped, field-induced ferromagnetic state [92]. In case of weak repulsion between spinons the divergence is associated with the onset of a topological transition at finite value of p_{FH} signaling that $M^*(T) \propto T^{-1/2}$. Thus, the bare interaction of spinons is weak [92]. In that case the original Tomonaga-Luttinger system [97–100] can exactly be mapped on a system of free spinons, which low-temperature behavior in magnetic fields can be viewed as the LFL one [101]. On the other hand, the fermion condensation associated with completely flat band does not occur as it is absorbed by gapped, field-induced ferromagnetic phase Fermi liquid at $H > H_s$ [92]. As a result, this new state at $H > H_s$ is protected by the gap rather than by the Volovik topological number [16, 18]. Nonetheless, at elevated temperatures the system bears fingerprints of FC with the behavior very similar to that of HF compounds with approximately flat bands [95, 96], including the LFL and NFL regimes. Note that recently a new state of matter, quasi-Fermi liquid, has been introduced by Rozhkov [102] in context of 1D Fermi liquid, while Lebed observed that applicability of Fermi-liquid theory restores in quasi-one-dimensional conductors [103]. This state exhibits, however, some of the properties of ordinary Fermi liquid accompanied by the NFL behavior. Thus $Cu(C_4H_4N_2)(NO_3)_2$ (CuPzN) offers a unique possibility to observe a new type of 1D quantum spin liquid whose thermodynamic properties resemble that of HF compounds. Theory of 1D liquids is still under construction and recent results show that the liquids can exhibit LFL, non-Fermi liquid (NFL) and crossover behavior [101–103].

Recent measurements on the insulator CuPzN [92] allow us to analyze the properties of 1D quantum spin liquid [95, 96]. In Fig. 14, panel (a), we compare our calculated χ_N with that extracted from measurements of the magnetization on single crystals of the insulator [92]. In order to understand the behavior of χ_N displayed in the panel (a) of Fig. 14, we contrast χ_N extracted from measurements [92] with that obtained on the QC $Au_{51}Al_{35}Yb_{14}$ displayed in the panel (b). It is seen from Fig. 14 that both the normalized χ_N shown in the panels (a) and (b) are in good agreement with each other. We now focus on the LFL, NFL and the crossover LFL-NFL regions exhibited by the normalized magnetic susceptibilities. To this end, we display in the panels (a) and (b) of Fig. 14 the normalized χ_N on the double logarithmic scale. As seen from Fig. 14, the two regions (the LFL and NFL regions) are clearly demarcated. And good agreement of theory with the experimental data is realized. The straight lines in Fig. 14, panels (a) and (b), capture both the LFL and NFL behaviors of $\chi_N \propto const$ and $\chi_N \propto T_N^{-1/2}$. These lines are in a good agreement with the behavior of M_N^* given by Eq. (11) with $n = 5/2$. Clearly, our calculations shown by the solid curve in the panel (a) agree well with the measurements over three orders of magnitude in the normalized temperature.

Taking into account that $M = \int \chi dH$ and Eqs. (11) and (13), we obtain that $(M_s - M)/\sqrt{H_s - H}$ as a function of the variable $T/(H_s - H)$ exhibits scaling behavior. Here M_s is the saturation magnetization, taking place at H_s. This result is in good agreement with the experimental facts, as it is seen from Fig. 15 that reports the plot of the scaling behavior of the magnetization $M_c/B^{0.5}$. In the case of CuPzN $M_c/B^{0.5}$ reads $M_c/B^{0.5} = a + (M_s - M)/(H_s - H)^{0.5}$, being a function of $T/B = T/(H_s - H)$, with a is a constant added to a better presentation of Fig. 15. In the case of β-$YbAlB_4$ magnetic field $H = B$ and M_c is taken from Refs. [52, 104]. It is seen from Fig. 15, that the LFL behavior takes place at $T \ll B$, the crossover at $T \sim B$, and the NFL one at $T \gg B$, as it is in the case of the HF superconductor β-$YbAlB_4$ [67], see Fig. 15, or the quasicrystal $Au_{51}Al_{34}Yb_{15}$, see Fig. 14 [54, 55]. We note that the observed NFL behavior of of CuPzN is

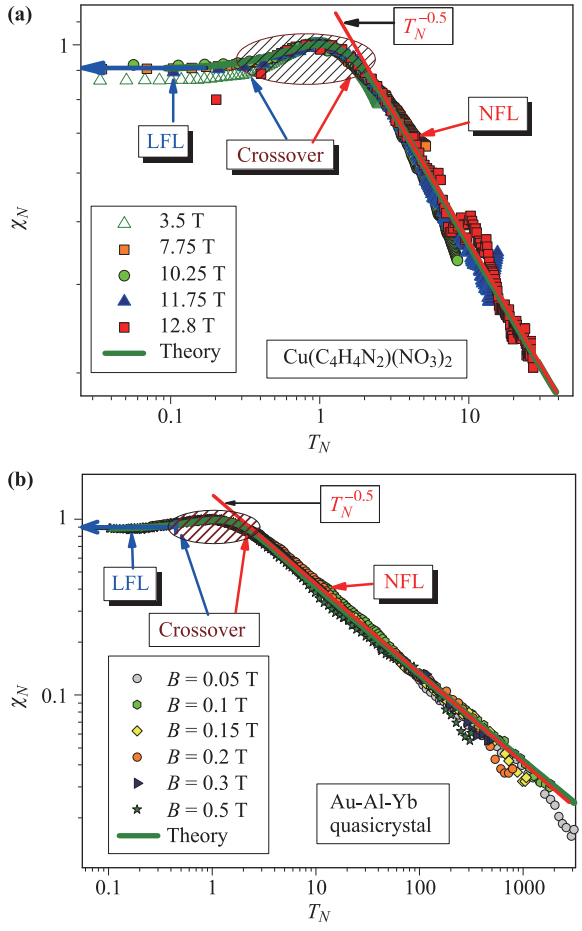

Fig. 14 Universal scaling behavior of both the insulator $Cu(C_4H_4N_2)(NO_3)_2$ with the 1D quantum spin liquid and the quasicrystal $Au_{51}Al_{35}Yb_{14}$. **(a)** Temperature dependence on the double logarithmic scale of the normalized magnetic susceptibility χ_N versus normalized temperature T_N, extracted from measurements of the magnetization on $Cu(C_4H_4N_2)(NO_3)_2$ at different magnetic fields [92] shown in the legend. The LFL and NFL regions are shown by the solid arrows. The crossover region is depicted by the shaded area. **(b)** Temperature dependence on the double logarithmic scale of the magnetic susceptibility χ_N, versus normalized temperature T_N, extracted from measurements of the magnetic susceptibility χ on the quasicrystal $Au_{51}Al_{35}Yb_{14}$ at different magnetic fields [54] shown in the legend. The LFL and NFL regions are shown by the arrows. The crossover region is depicted by the two arrows and dashed area. The solid line marked by the NFL displays $M_N^* \propto T_N^{-0.5}$ behavior. In both panels, our calculations are shown by the same solid curve taken from Fig. 13.

extremely sensitive to a magnetic field, as it is in the case of both $Au_{51}Al_{34}Yb_{15}$ and β-$YbAlB_4$. It is worthy of note that the scaling behavior of the thermodynamic properties of CuPzN has been observed in Ref. [105].

As a result, we conclude that 1D quantum spin liquid of the insulator $Cu(C_4H_4N_2)(NO_3)_2$ exhibits the typical

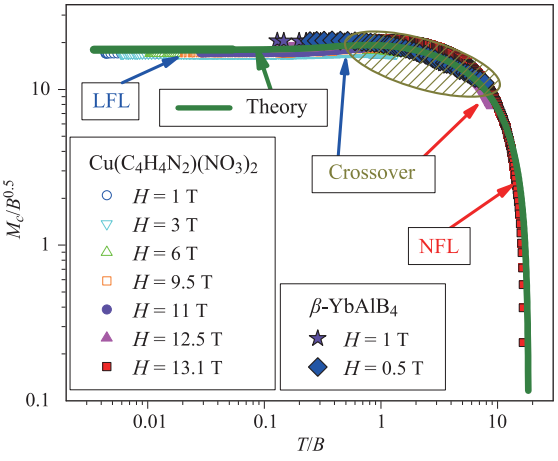

Fig. 15 The scaling dependence of $M_c/B^{0.5}$ versus T/B for CuPzN and HF superconductor β-$YbAlB_4$. Here, $B = H_s - H$, see text for details. The experimental data are taken from Refs. [52, 92, 104] and normalized making them merge in the LFL region. The curves corresponding to different magnetic fields H are shown in the legends. The LFL, crossover and NFL regions are shown. The theory is depicted by the solid curve [95].

scaling behavior of its thermodynamic properties, and belongs to the famous family of HF compounds, and therefore forms the new state of matter [95, 96]. Thus, we expect the quantum physics of the 1D quantum spin liquid to be universal, and to emerge regardless of the underlying microscopic details of insulators holding the liquid.

7 Summary

We have shown both analytically and using arguments based entirely on the experimental facts that the data collected on very different strongly correlated Fermi systems named HF compounds and represented by HF metals, quantum liquids like 2D ^{3}He, insulators with 2D, 3D quantum spin liquids and 1D quantum spin liquids, and quasicrystals, have the universal scaling behavior, observed in their thermodynamic, transport and relaxation properties. Thus, despite of their drastic microscopic diversity, strongly correlated Fermi systems exhibit the uniform scaling behavior. The quantum physics of different strongly correlated Fermi systems is universal and emerges regardless of their underlying microscopic details. The observed behavior resembles the uniform collective behavior exhibited by such different states of matter as the gaseous, liquid and solid states of matter. Therefore, this uniform behavior, formed by flat bands, allows us to view it as the main manifestation of the new state of matter exhibited by HF compounds.

Acknowledgements V. R. Shaginyan is supported by the Russian Science Foundation, Grant No. 14-22-00281. A. Z. Msezane thanks the US DOE, Division of Chemical Sciences, Office of Energy Research, and ARO for research support. K. G. Popov is partly supported by RFBR # 14-02-00044. V. A. Khodel thanks the McDonnell Center for the Space Sciences for support.

References and notes

1. L. D. Landau, The theory of a Fermi liquid, *Sov. Phys. JETP* 3(6), 920 (1957)
2. L. D. Landau, On the theory of the Fermi liquid, *Sov. Phys. JETP* 8(1), 70 (1959)
3. E. M. Lifshitz and L. P. Pitaevskii, Statistical Physics, Part 2, Oxford: Pergamon Press, 1980
4. V. R. Shaginyan, M. Ya. Amusia, A. Z. Msezane, and K. G. Popov, Scaling behavior of heavy-fermion metals, *Phys. Rep.* 492(2–3), 31 (2010)
5. M. Ya. Amusia, K. G. Popov, V. R. Shaginyan, and W. A. Stephanowich, Theory of Heavy-Fermion Compounds, Solid-State Sciences 182, Springer, Heidelberg, New York, Dordrecht, London, 2015
6. V. A. Khodel, V. R. Shaginyan, and V. V. Khodel, New approach in the microscopic Fermi systems theory, *Phys. Rep.* 249(1–2), 1 (1994)
7. V. R. Shaginyan, Universal behavior of heavy-fermion metals near a quantum critical point, *JETP Lett.* 79(6), 286 (2004)
8. I. Ya. Pomeranchuk, On the stability of a Fermi liquid, *Sov. Phys. JETP* 8(2), 361 (1959)
9. P. Noziéres, Properties of Fermi liquids with a finite range interaction, J. Phys. I France 2(4), 443 (1992)
10. A. Casey, H. Patel, J. Nyeki, B. P. Cowan, and J. J. Saunders, Strongly correlated two dimensional fluid ^{3}He, *Low Temp. Phys.* 113(3), 293 (1998)
11. M. Neumann, J. Nyéki, B. Cowan, and J. Saunders, Bilayer ^{3}He: A simple two-dimensional heavy-fermion system with quantum criticality, *Science* 317(5843), 1356 (2007)
12. V. R. Shaginyan, A. Z. Msezane, K. G. Popov, and V. A. Stephanovich, Universal behavior of two-dimensional 3He at low temperatures, *Phys. Rev. Lett.* 100(9), 096406 (2008)
13. P. Hohenberg and W. Kohn, Inhomogeneous electron gas, *Phys. Rev.* 136(3B), B864 (1964)
14. W. Kohn and L. J. Sham, Self-consistent equations including exchange and correlation effects, *Phys. Rev.* 140(4A), A1133 (1965)
15. V. A. Khodel and V. R. Shaginyan, Superfluidity in system with fermion condensate, *JETP Lett.* 51(9), 553 (1990)
16. G. E. Volovik, A new class of normal Fermi liquids, *JETP Lett.* 53(4), 222 (1991)
17. G. E. Volovik, T. T. Heikkilá, and N. B. Kopnin, Flat bands in topological media, *JETP Lett.* 94(3), 252 (2011)
18. G. E. Volovik, From standard model of particle physics to room-temperature superconductivity, *Phys. Scr.* 215(T164), 014014 (2015)
19. T. T. Heikkilá and G. E. Volovik, Flat bands as a route to high-temperature superconductivity in graphite, arxiv: 1504.05824, submitted as a chapter to the book on Basic Physics of functionalized Graphite
20. M. Ya. Amusia and V. R. Shaginyan, Fermion condensate as a new state of matter, *Contrib. Plasma Phys.* 53(10), 721 (2013)
21. D. Yudin, D. Hirschmeier, H. Hafermann, O. Eriksson, A. I. Lichtenstein, and M. I. Katsnelson, Fermi condensation near van Hove singularities within the Hubbard model on the triangular lattice, *Phys. Rev. Lett.* 112(7), 070403 (2014)
22. M. V. Zverev, V. A. Khodel, V. R. Shaginyan, and M. Baldo, Critical experiments in the search for fermion condensation, *JETP Lett.* 65(11), 863 (1997)
23. H. Löhneysen, Non-Fermi-liquid behaviour in the heavy-fermion system $CeCu_{1-x}Au_x$, *J. Phys.: Condens. Matter* 8(48), 9689 (1996)
24. V. R. Shaginyan, M. Ya. Amusia, and K. G. Popov, Behavior of the antiferromagnetic phase transition near the fermion condensation quantum phase transition in $YbRh_2Si_2$, *Phys. Lett. A* 374(4), 659 (2010)
25. D. Lidsky, J. Shiraishi, Y. Hatsugai, and M. Kohmoto, Simple exactly solvable models of non-Fermi-liquids, *Phys. Rev. B* 57(3), 1340 (1998)
26. V. Yu. Irkhin, A. A. Katanin, and M. I. Katsnelson, Robustness of the Van Hove Scenario for high-T_c superconductors, *Phys. Rev. Lett.* 89(7), 076401 (2002)
27. S. S. Lee, Non-Fermi liquid from a charged black hole: A critical Fermi ball, *Phys. Rev. D* 79(8), 086006 (2009)
28. A. A. Shashkin, V. T. Dolgopolov, J. W. Clark, V. R. Shaginyan, M. V. Zverev, and V. A. Khodel, Merging of Landau levels in a strongly-interacting two-dimensional electron system in silicon, *Phys. Rev. Lett.* 112(18), 186402 (2014)
29. M. Yu. Melnikov, A. A. Shashkin, V. T. Dolgopolov, S.H. Huang, C. W. Liu, and S. V. Kravchenko, Indication of the fermion condensation in a strongly correlated electron system in SiGe/Si/SiGe quantum wells, arXiv: 1604.08527
30. V. A. Khodel, J. W. Clark, and M. V. Zverev, Topology of the Fermi surface beyond the quantum critical point, *Phys. Rev. B* 78(7), 075120 (2008)
31. S. A. Artamonov, V. R. Shaginyan, and Yu. G. Pogorelov, Ground-state instability in systems of strongly interacting fermions, *JETP Lett.* 68(12), 942 (1998)
32. V. A. Khodel, Two scenarios of the quantum critical point, *JETP Lett.* 86(11), 721 (2008)

33. N. Oeschler, S. Hartmann, A. P. Pikul, C. Krellner, C. Geibel, and F. Steglich, Low-temperature specific heat of $YbRh_2Si_2$, *Physica B* 403(5–9), 1254 (2008)

34. V. R. Shaginyan, M. Ya. Amusia, and K. G. Popov, Strongly correlated Fermi-systems: Non-Fermi liquid behavior, quasiparticle effective mass and their interplay, *Phys. Lett. A* 373(26), 2281 (2009)

35. M. Brando, L. Pedrero, T. Westerkamp, C. Krellner, P. Gegenwart, C. Geibel, and F. Steglich, Magnetization study of the energy scales in $YbRh_2Si_2$ under chemical pressure, *Phys. Status Solidi B* 250(3), 485 (2013)

36. V. R. Shaginyan, A. Z. Msezane, K. G. Popov, G. S. Japaridze, and V. A. Khodel, General properties of phase diagrams of heavy-fermion metals, *Europhys. Lett.* 106(3), 37001 (2014)

37. D. Takahashi, S. Abe, H. Mizuno, D. A. Tayurskii, K. Matsumoto, H. Suzuki, and Y. Onuki, ac susceptibility and static magnetization measurements of $CeRu_2Si_2$ at small magnetic fields and ultralow temperatures, *Phys. Rev. B* 67(18), 180407 (2003)

38. A. W. Rost, S. A. Grigera, J. A. N. Bruin, R. S. Perry, D. Tian, S. Raghu, S. A. Kivelson, and A. P. Mackenzie, Thermodynamics of phase formation in the quantum critical metal $Sr_3Ru_2O_7$, *Proc. Natl. Acad. Sci. USA* 108(40), 16549 (2011)

39. A. V. Silhanek, N. Harrison, C. D. Batista, M. Jaime, A. Lacerda, H. Amitsuka, and J. A. Mydosh, Quantum critical 5f electrons avoid singularities in $U(Ru; Rh)_2Si_2$, *Phys. Rev. Lett.* 95(2), 026403 (2005)

40. J. S. Kim, B. Andraka, G. Fraunberger, and G. R. Stewart, Specific heat in a magnetic field: A probe of the magnetic ground-state properties of heavy-fermion $Ce(Ru_{2-x}Rh_x)Si2_{2-y}Ge_y$, *Phys. Rev. B* 41(1), 541 (1990)

41. V. R. Shaginyan, K. G. Popov, V. A. Stephanovich, V. I. Fomichev, and E. V. Kirichenko, High magnetic fields thermodynamics of heavy fermion metal $YbRh_2Si_2$, *Europhys. Lett.* 93(1), 17008 (2011)

42. P. Gegenwart, Y. Tokiwa, T. Westerkamp, F. Weickert, J. Custers, J. Ferstl, C. Krellner, C. Geibel, P. Kerschl, K-H. Müller, and F. Steglich, High-field phase diagram of the heavy-fermion metal $YbRh_2Si_2$, *New J. Phys.* 8(9), 171 (2006)

43. H. Löhneysen, A. Rosch, M. Vojta, and P. Wölfle, Fermi-liquid instabilities at magnetic quantum phase transitions, *Rev. Mod. Phys.* 79(3), 1015 (2007)

44. P. Coleman, C. Pépin, Q. Si, and R. Ramazashvili, How do Fermi liquids get heavy and die? *J. Phys.: Condens. Matter* 13(35), R723 (2001)

45. J. Custers, P. Gegenwart, H. Wilhelm, K. Neumaier, Y. Tokiwa, O. Trovarelli, C. Geibel, F. Steglich, C. Pépin, and P. Coleman, C. Pépin, and P. Coleman, The break-up of heavy electrons at a quantum critical point, *Nature* 424(6948), 524 (2003)

46. S. Paschen, T. Lühmann, S. Wirth, P. Gegenwart, O. Trovarelli, C. Geibel, F. Steglich, P. Coleman, and Q. Si, Hall-effect evolution across a heavy fermion quantum critical point, *Nature* 432(7019), 881 (2004)

47. Y. Yang, Z. Fisk, H-O. Lee, J. D. Thompson, and D. Pines, Scaling the Kondo lattice, *Nature* 454(7204), 611 (2008)

48. Y. Yang and D. Pines, Universal behavior in heavy-electron materials, *Phys. Rev. Lett.* 100(9), 096404 (2008)

49. Y. Yang and D. Pines, Quantum critical behavior in heavy electron materials, *Proc. Natl. Acad. Sci. USA* 111(23), 8398 (2014)

50. P. Wölfle and E. Abrahams, Quasiparticles beyond the Fermi liquid and heavy fermion criticality, *Phys. Rev. B* 84(4), 041101(R) (2011)

51. E. Abrahams and P. Wölfle, Critical quasiparticle theory applied to heavy fermion metals near an antiferromagnetic quantum phase transition, *Proc. Natl. Acad. Sci. USA* 109(9), 3238 (2012)

52. Y. Matsumoto, S. Nakatsuji, K. Kuga, Y. Karaki, N. Horie, Y. Shimura, T. Sakakibara, A. H. Nevidomskyy, and P. Coleman, Quantum Criticality Without Tuning in the Mixed Valence Compound β-$YbAlB_4$, *Science* 331(6015), 316 (2011)

53. T. Tomita, K. Kuga, Y. Uwatoko, P. Coleman, and S. Nakatsuji, Strange metal without magnetic criticality, *Science* 349(6247), 506 (2015)

54. K. Deguchi, S. Matsukawa, N. K. Sato, T. Hattori, K. Ishida, H. Takakura, and T. Ishimasa, Quantum critical state in a magnetic quasicrystal, *Nat. Mater.* 11(12), 1013 (2012)

55. V. R. Shaginyan, A. Z. Msezane, K. G. Popov, G. S. Japaridze, and V. A. Khodel, Common quantum phase transition in quasicrystals and heavy-fermion metals, *Phys. Rev. B* 87(24), 245122 (2013)

56. V. R. Shaginyan, A. Z. Msezane, K. G. Popov, J. W. Clark, V. A. Khodel, and M. V. Zverev, Topological basis for understanding the behavior of the heavy-fermion metal β-YbAlB4 under application of magnetic field and pressure, *Phys. Rev. B* 93(20), 205126 (2016)

57. K. S. Kim and C. Pépin, Thermopower as a signature of quantum criticality in heavy fermions, *Phys. Rev. B* 81(20), 205108 (2010)

58. K. S. Kim and C. Pépin, Thermopower as a fingerprint of the Kondo breakdown quantum critical point, *Phys. Rev. B* 83(7), 073104 (2011)

59. K. Behnia, D. Jaccard, and J. Flouquet, On the thermoelectricity of correlated electrons in the zero-temperature limit, *J. Phys.: Condens. Matter* 16(28), 5187 (2004)

60. K. Miyake and H. Kohno, Theory of quasi-universal ratio of Seebeck coefficient to specific heat in zero-temperature limit in correlated metals, *J. Phys. Soc. Jpn.* 74(1), 254 (2005)

61. V. Zlatić R. Monnier, J. K. Freericks, and K. W. Becker, Relationship between the thermopower and entropy of strongly correlated electron systems, *Phys. Rev. B* 76(8), 085122 (2007)

62. S. Hartmann, N. Oeschler, C. Krellner, C. Geibel, S. Paschen, and F. Steglich, Thermopower evidence for an abrupt Fermi surface change at the quantum critical point of $YbRh_2Si_2$, *Phys. Rev. Lett.* 104(9), 096401 (2010)

63. S. Friedemann, S. Wirth, S. Kirchner, Q. Si, S. Hartmann, C. Krellner, C. Geibel, T. Westerkamp, M. Brando, and F. Steglich, Break up of heavy fermions at an antiferromagnetic instability, *J. Phys. Soc. Jpn.* 80(10 Suppl.A), SA002 (2011)

64. P. Gegenwart, J. Custers, C. Geibel, K. Neumaier, T. Tayama, K. Tenya, O. Trovarelli, and F. Steglich, Magnetic-field induced quantum critical point in $YbRh_2Si_2$, *Phys. Rev. Lett.* 89(5), 056402 (2002)

65. A. Mokashi, S. Li, B. Wen, S. V. Kravchenko, A. A. Shashkin, V. T. Dolgopolov, and M. P. Sarachik, Critical behavior of a strongly interacting 2D electron system, *Phys. Rev. Lett.* 109(9), 096405 (2012)

66. Y. Machida, K. Tomokuni, C. Ogura, K. Izawa, K. Kuga, S. Nakatsuji, G. Lapertot, G. Knebel, J. P. Brison, and J. Flouquet, Thermoelectric response near a quantum critical point of $YbAlB_4$ and $YbRh_2Si_2$: A comparative study, *Phys. Rev. Lett.* 109(15), 156405 (2012)

67. V. R. Shaginyan, A. Z. Msezane, G. S. Japaridze, K. G. Popov, J. W. Clark, and V. A. Khodel, Scaling behavior of the thermopower of the archetypal heavy-fermion metal $YbRh_2Si_2$, *Front. Phys.* 11(2), 117102 (2016)

68. P. Limelette, W. Saulquin, H. Muguerra, and D. Grebille, From quantum criticality to enhanced thermopower in strongly correlated layered cobalt oxide, *Phys. Rev. B* 81(11), 115113 (2010)

69. T. H. Han, J. S. Helton, S. Chu, D. G. Nocera, J. A. Rodriguez-Rivera, C. Broholm, and Y. S. Lee, Fractionalized excitations in the spin-liquid state of a kagome-lattice antiferromagnet, *Nature* 492(7429), 406 (2012)

70. P. Mendels and F. Bert, Quantum kagome antiferromagnet $ZnCu_3(OH)_6Cl_2$, *J. Phys. Soc. Jpn.* 79(1), 011001 (2010)

71. D. Green, L. Santos, and C. Chamon, Isolated flat bands and spin-1 conical bands in two-dimensional lattices, *Phys. Rev. B* 82(7), 075104 (2010)

72. T. H. Han, S. Chu, and Y. S. Lee, Refining the spin hamiltonian in the spin-1/2 kagome lattice antiferromagnet $ZnCu_3(OH)_6Cl_2$ using single crystals, *Phys. Rev. Lett.* 108(15), 157202 (2012)

73. M. A. de Vries, K. V. Kamenev, W. A. Kockelmann, J. Sanchez-Benitez, and A. Harrison, Magnetic ground state of an experimental $S = 1/2$ kagome antiferromagnet, *Phys. Rev. Lett.* 100(15), 157205 (2008)

74. V. R. Shaginyan, A. Z. Msezane, K. G. Popov, G. S. Japaridze, and V. A. Stephanovich, Identification of strongly correlated spin liquid in herbertsmithite, *Europhys. Lett.* 97(5), 56001 (2012)

75. V. R. Shaginyan, A. Z. Msezane, and K. G. Popov, Thermodynamic properties of the kagome lattice in herbertsmithite, *Phys. Rev. B* 84(6), 060401(R) (2011)

76. V. R. Shaginyan, A. Z. Msezane, K. G. Popov, and V. A. Khodel, Scaling in dynamic susceptibility of herbertsmithite and heavy-fermion metals, *Phys. Lett. A* 376(38–39), 2622 (2012)

77. V. R. Shaginyan, A. Z. Msezane, K. G. Popov, and V. A. Stephanovich, Magnetic-field-induced reentrance of fermi-liquid behavior and spin-lattice relaxation rates in $YbCu_{5-x}Au_x$, *Phys. Lett. A* 373(41), 3783 (2009)

78. T. Imai, E. A. Nytko, B. M. Bartlett, M. P. Shores, and D. G. Nocera, ^{63}Cu, ^{35}Cl, and ^{1}H NMR in the $S = 1/2$ kagome lattice $ZnCu_3(OH)_6Cl_2$, *Phys. Rev. Lett.* 100(7), 077203 (2008)

79. P. Carretta, R. Pasero, M. Giovannini, and C. Baines, Magnetic-field-induced crossover from non-Fermi to Fermi liquid at the quantum critical point of $YbCu_{5-x}Au_x$, *Phys. Rev. B* 79(2), 020401 (2009)

80. P. Gegenwart, T. Westerkamp, C. Krellner, Y. Tokiwa, S. Paschen, C. Geibel, F. Steglich, E. Abrahams, and Q. Si, Multiple energy scales at a quantum critical point, *Science* 315(5814), 969 (2007)

81. J. S. Helton, K. Matan, M. P. Shores, E. A. Nytko, B. M. Bartlett, Y. Qiu, D. G. Nocera, and Y. S. Lee, Dynamic scaling in the susceptibility of the spin-1/2 kagome lattice antiferromagnet herbertsmithite, *Phys. Rev. Lett.* 104(14), 147201 (2010)

82. V. R. Shaginyan, A. Z. Msezane, K. G. Popov, G. S. Japaridze, and V. A. Khodel, Heat transport in magnetic fields by quantum spin liquid in the organic insulators $EtMe_3Sb[Pd(dmit)_2]_2$ and κ-(BEDT-TTF)$_2Cu_2(CN)_3$, *Europhys. Lett.* 103(6), 67006 (2013)

83. M. Yamashita, N. Nakata, Y. Senshu, M. Nagata, H. M. Yamamoto, R. Kato, T. Shibauchi, and Y. Matsuda, Highly mobile gapless excitations in a two-dimensional candidate quantum spin liquid, *Science* 328(5983), 1246 (2010)

84. M. Yamashita, T. Shibauchi, and Y. Matsuda, Thermal-transport studies of two-dimensional quantum spin liquids, *ChemPhysChem* 13(1), 74 (2012)

85. W. Knafo, S. Raymond, J. Flouquet, B. Fåk, M. A. Adams, P. Haen, F. Lapierre, S. Yates, and P. Lejay, Anomalous scaling behavior of the dynamical spin susceptibility of $Ce_{0:925}La_{0:075}Ru_2Si_2$, *Phys. Rev. B* 70(17), 174401 (2004)

86. B. Fåk, F. C. Coomer, A. Harrison, D. Visser, and M. E. Zhitomirsky, Spin-liquid behavior in a kagome antiferromagnet: Deuteronium jarosite, *Europhys. Lett.* 81(1), 17006 (2008)

87. V. R. Shaginyan, K. G. Popov, and V. A. Khodel, Strongly correlated quantum spin liquid in herbertsmithite, *Sov. Phys. JETP* 116(5), 848 (2013)

88. D. Shechtman, I. Blech, D. Gratias, and J. W. Cahn, Metallic phase with long-range orientational order and no translational symmetry, *Phys. Rev. Lett.* 53(20), 1951 (1984)

89. T. Fujiwara, *Theory of Electronic Structure in Quasicrystals* 126, Springer Series in Solid-State Sciences, Berlin: Springer-Verlag, 1999

90. R. Widmer, P. Gröning, M. Feuerbacher, and O. Gröning, Experimental signatures of spiky local density of states in quasicrystals, *Phys. Rev. B* 79(10), 104202 (2009)

91. G. T. de Laissardiere, Spiky density of states in large complex Al-Mn phases, *Zeitschrift für Kristallographie - Crystalline Materials* 224(1–2), 123 (2009)

92. Y. Kono, T. Sakakibara, C. P. Aoyama, C. Hotta, M. M. Turnbull, C. P. Landee, and Y. Takano, Field-induced quantum criticality and universal temperature dependence of the magnetization of a spin-1/2 Heisenberg chain, *Phys. Rev. Lett.* 114(3), 037202 (2015)

93. V. A. Khodel, J. W. Clark, and M. V. Zverev, Superfluid phase transitions in dense neutron matter, *Phys. Rev. Lett.* 87(3), 031103 (2001)

94. V. R. Shaginyan, G. S. Japaridze, M. Ya. Amusia, A. Z. Msezane, and K. G. Popov, Baryon asymmetry resulting from a quantum phase transition in the early universe, *Europhys. Lett.* 94(6), 69001 (2011)

95. V. R. Shaginyan, V. A. Stephanovich, K. G. Popov, and E. V. Kirichenko, Quasi-one-dimensional quantum spin liquid in the $Cu(C_4H_4N_2)(NO_3)_2$ insulator, *JETP Lett.* 103(1), 30 (2016)

96. V. R. Shaginyan, V. A. Stephanovich, K. G. Popov, E. V. Kirichenko, and S. A. Artamonov, *Magnetic quantum criticality in quasi-one-dimensional Heisenberg* antiferromagnet $Cu(C_4H_4N_2)(NO_3)_2$, *Ann. Phys. (Berlin)*, 528(6), 483 (2016)

97. S. Tomonaga, Remarks on Bloch's method of sound waves applied to many-fermion problems, *Prog. Theor. Phys.* 5(4), 544 (1950)

98. J. M. Luttinger, An exactly soluble model of a many-fermion system, *Math. Phys.* 4(9), 1154 (1963)

99. F. D. M. Haldane, Luttinger liquid theory of one-dimensional quantum fluids. I. Properties of the Luttinger model and their extension to the general 1D interacting spinless Fermi gas, *J. Phys. C* 14(19), 2585 (1981)

100. F. D. M. Haldane, General relation of correlation exponents and spectral properties of one-dimensional fermi systems: Application to the anisotropic $S = 1/2$ Heisenberg chain, *Phys. Rev. Lett.* 45(16), 1358 (1980)

101. A. V. Rozhkov, Fermionic quasiparticle representation of Tomonaga-Luttinger Hamiltonian, *Eur. Phys. J. B* 47(2), 193 (2005)

102. A. V. Rozhkov, One-dimensional fermions with neither Luttinger-liquid nor Fermi-liquid behavior, *Phys. Rev. Lett.* 112(10), 106403 (2014)

103. A. G. Lebed, Non-Fermi-liquid crossovers in a quasi one-dimensional conductor in a tilted magnetic fleld, *Phys. Rev. Lett.* 115(15), 157001 (2015)

104. Y. Matsumoto, S. Nakatsuji, K. Kuga, Y. Karaki, Y. Shimura, T. Sakakibara, A. H. Nevidomskyy, and P. Coleman, T/B scaling of magnetization in the mixed valent compound β-$YbAlB_4$, *J. Phys. Conf. Ser.* 391(1), 012041 (2012)

105. M. Jeong and H. M. Rónnow, Quantum critical scaling for a Heisenberg spin-1/2 chain around saturation, *Phys. Rev. B* 92(18), 180409(R) (2015)